Dirk Kehrwald

Numerical Simulation of a Channel Inflow with Moving Contact Lines

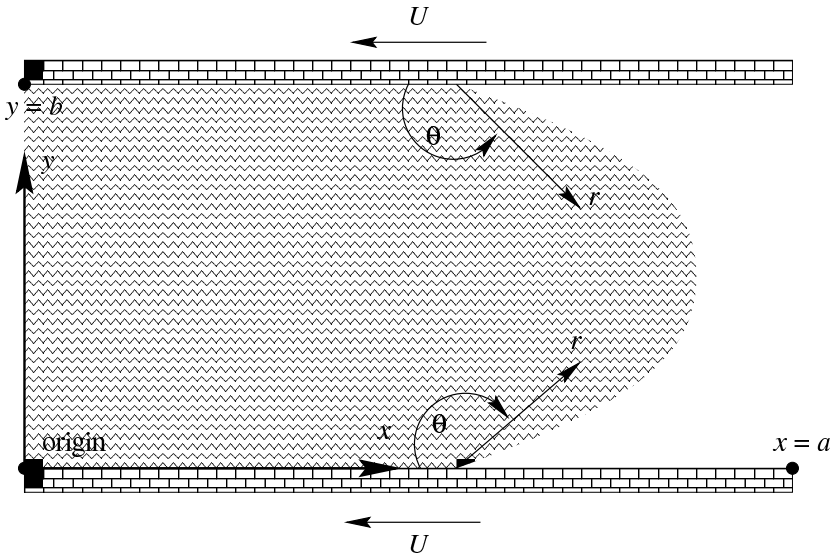

UNIVERSITÄT
KAISERSLAUTERN

Dirk Kehrwald

Numerical Simulation of a Channel Inflow with Moving Contact Lines

A thesis submitted for the grade of
Diplom–Technomathematiker (Dipl.–Math. techn.)
in the Mathematical Department of the
University of Kaiserslautern, Germany

9th November 1998

Acknowledgements

I want to thank Prof. Dr. Helmut Neunzert for initiating this very interesting thesis, Dr. Holger Seguin for introducing me to modern numerical methods for free surface flow and supervising the first period of this thesis, and Priv.–Doz. Dr. Jens Struckmeier for supervising the second period, drawing my attention to the essential aspects of the topic, reading the manuscript, and giving many helpful hints. Furthermore, I am very grateful to many of my fellow students for lots of helpful hints and fruitful discussions.

Last, but not at all least, I want to express my deep gratitude to my girl–friend Dagmar Ernst and my family for all their love and understanding, and their support during my studies.

Kaiserslautern, 9th November 1998

Dirk Kehrwald

Table of Contents

Acknowledgements **2**

Table of Contents **3**

List of Figures **5**

1 Introduction **6**
1.1 The Moving Contact Line Problem 6
1.2 The Approach 7

2 The Mathematical Model **9**
2.1 The General Formulation 9
2.2 Simplification of the Conditions at the Free Liquid Surface 13
2.3 Summary of the Model Equations 14
2.4 Nondimensionalization 15
2.4.1 The Navier–Stokes Equations 15
2.4.2 The Conditions at the Solid Surface 17
2.4.3 The Conditions at the Free Surface 19
2.4.4 Summary of the Dimensionless Equations 20
2.5 Steady Flow with $Re, Ca, \epsilon \to 0$ 21
2.6 The 'Outer' Region 23
2.7 The Slip Region 28
2.7.1 The Governing Equations 28
2.7.2 The Boundary Conditions for the Slip Region 33
2.7.3 The Constant of Integration 36
2.8 The Dynamic Contact Angle 38
2.9 Summary of the Results 38

3 The Numerical Method **41**
3.1 On the Implementation of the Model into the Existing Code . . . 41
3.2 The Computational Grid 43
3.3 The Treatment of the Stokes Equations 44
3.3.1 The Discretization 46

3.3.2 The Solution Scheme 47
3.3.3 The Poisson Equation for p 50
3.4 The Treatment of the Free Liquid Surface 54
3.5 The Boundary Conditions for the Flow Field 57
3.5.1 The 'Inflow' Boundary 58
3.5.2 Solid Boundaries of the Bulk 59
3.5.3 The Slip Region 59
3.5.4 The Free Surface of the Bulk and the 'Outflow' Boundary 60
3.6 The Basic Features of the Problem Solver 60
3.6.1 The Problem Parameters 60
3.6.2 A Sketch of the Complete Algorithm 63

4 Some Numerical Results **64**
4.1 On an 80×20 Grid 65
4.2 On a 160×40 Grid 68
4.3 The Behaviour of the Numerical Method 72

5 Concluding Remarks **74**
5.1 What Could Be Done 74
5.2 What Could not Be Done 74

A Notations **76**
A.1 A List of Operators 76
A.2 A List of Symbols 77

Bibliography **82**

List of Figures

1.1 The geometry of a flow system where liquid is flowing into an empty channel 7
1.2 The rolling motion of the liquid in the vicinity of the moving contact line 7

2.1 A solid is moving with speed U along an interface between a liquid and an ideal, inviscid gas 10
2.2 The interfacial layer adjacent to the boundary 10
2.3 The asymptotic regions around the contact line 22
2.4 The co–ordinate frame (r, θ) 24

3.1 Channel flow with two moving contact lines 42
3.2 The asymptotic regions inside the channel 42
3.3 The co–ordinate system used for the numerical method presented in this chapter 44
3.4 The staggered grid 45
3.5 The computational domain including the ghost layer 45
3.6 The quantities needed for the Bézier method 55
3.7 The exact shape of the free liquid surface and its approximation by cell edges 57
3.8 The numerical slip regions inside the channel 58

4.1 The velocity field computed on an 80×20 grid 65
4.2 u computed on an 80×20 grid 66
4.3 v computed on an 80×20 grid 66
4.4 The pressure distribution computed on an 80×20 grid 67
4.5 The evaluation of u on a 80×20 grid 67
4.6 The evaluation of v on a 80×20 grid 68
4.7 The velocity field computed on a 160×40 grid 69
4.8 u computed on a 160×40 grid 69
4.9 v computed on a 160×40 grid 70
4.10 The pressure distribution computed on a 160×40 grid 70
4.11 The evaluation of u on a 160×40 grid 71
4.12 The evaluation of v on a 160×40 grid 71

Chapter 1

Introduction

In this thesis, we will consider the flow of a liquid into an empty channel surrounded by solid walls, as shown in Figure 1.1. The motivation to investigate this channel inflow is the wish to be able to simulate filling processes in foundries, i.e. to simulate liquid steel flowing into forms. This thesis is a first step towards the solution of this very complicated problem.

1.1 The Moving Contact Line Problem

The main difficulty arising in the simulation of channel inflow is the intersection of the free liquid surface with the solid boundaries of the liquid domain. Such an intersection is called a contact line. (Please note that in a plane co–ordinate frame, the contact line reduces to a single point. However, most authors use the term contact line even in this case, and we will do so as well in this thesis.) Since we will consider a liquid in motion, the contact line will change its position with respect to the channel, and therefore we will face a problem known in the literature as the moving contact line problem. The main feature of the moving contact line problem is that using the classical no–slip boundary condition at the solid boundaries and the classical zero tangential stress boundary condition at the free liquid surface will lead to a non–integrable singularity of the shear stress at the moving contact line, and therefore to an infinite force exerted by the liquid on the solid, as well as to a pressure singularity at the same location. Even if we decide to ignore this problem and to compose a numerical method for the computation of the flow field without taking care about the shear stress problem, we will find that the contact line always sticks to the solid at its initial position while the liquid bulk is in motion. As well as the shear stress singularity, this is not at all acceptable from a physical point of view, and so we really have to take care of the moving contact line problem. A list of papers considering this problem can be found in §9 of [15].

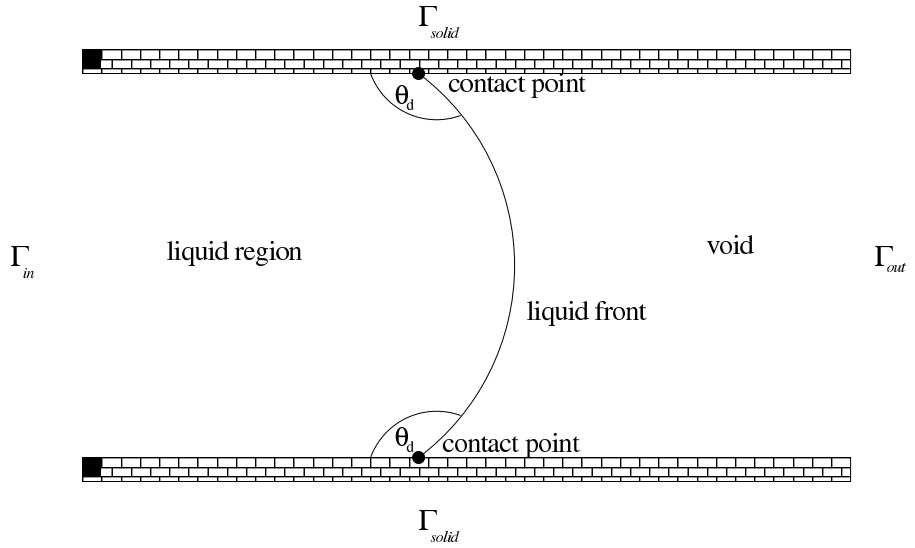

FIGURE 1.1: The geometry of a flow system where liquid is flowing into an empty channel

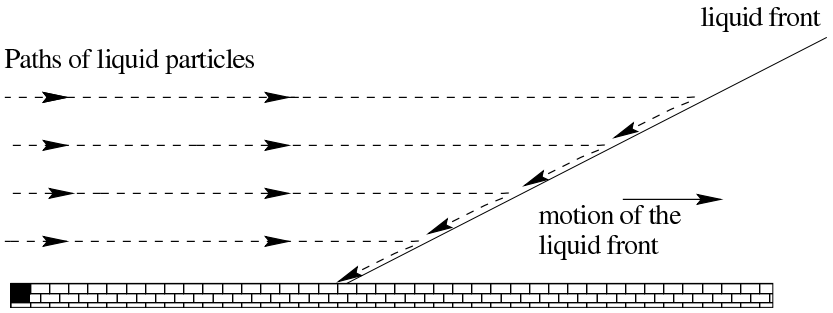

FIGURE 1.2: The rolling motion of the liquid in the vicinity of the moving contact line

1.2 The Approach

This thesis is based on a theory for flow with moving contact lines developed recently by Y. D. Shikhmurzaev [13, 14, 15]. The basic features of this theory will be outlined in this section.

From experimental studies, we know the following facts about advancing contact lines [13]:

(i) The free surface velocity directed towards the contact line is greater than the velocity in the bulk, and material points initially located at the free liquid surface will arrive at the solid boundary of the liquid domain after finite time. Therefore, we will denote the spreading of the liquid over the solid surface as rolling (see Figure 1.2).

(ii) With increasing contact line speed, the dynamic contact angle θ_d (which is the angle between the free and the solid boundary of the liquid domain when the liquid is in motion) is growing from the static contact angle θ_s (which is the angle between the free and the solid boundary of the liquid domain when the liquid is in rest) up to some limiting value θ_{max}.

(iii) The value of θ_{max} depends on the contacting media, and most gas/liquid/solid systems have a limiting contact angle equal or very close to 90^o, but for some of them it is considerably less.

(iv) At a certain contact line speed depending on the contacting materials the contact line motion becomes unstable (see [2, 3, 8] for details).

The aim of Shikhmurzaev was to give a model which eliminates the shear stress singularity and describes the qualitative features of the above phenomena. This model is based on the following physical ideas:

- Due to the true kinematics of the flow (see (i)), liquid elements from the free surface traverse the contact line in finite time, and therefore their surface properties have to relax to new equilibrium values giving rise to surface tension gradients in the immediate neighborhood of the advancing contact line.

- The deviation of the dynamic contact angle θ_d away from the static contact angle θ_s (see (ii)) together with the tangential momentum balance law (the classical Young equation (2.181)) also imply that the surface tensions along the free and solid boundaries are not in equilibrium in the vicinity of the moving contact line.

- The surface tension relaxation occurs not at the moving contact line but along the liquid–void and liquid–solid interfaces.

- The surface tension gradients along the interfaces in the vicinity of the moving contact line are caused by the flow and will have the reverse influence on the flow which caused them.

The resulting mathematical model is very complicated in its general formulation, but under certain conditions it can be considerably simplified by using perturbation methods. The model is valid for general fluid/liquid/solid systems [15], i.e. flow systems where a liquid replaces some arbitrary fluid along a solid, but due to the nature of our physical problem we will only look at the special case of a void/liquid/solid system, where we will approximate void as a dynamically passive, inviscid gas.

Chapter 2

The Mathematical Model

The aim of this chapter is to give an overview of the mathematical model for flow with a moving contact line as developed recently by Shikhmurzaev [13, 14, 15]. Therefore, we will have a look at a plane solid moving with speed U along an interface between a liquid and an ideal, inviscid gas, as shown in Figure 2.1. We will give the general formulation of the model (Section 2.1), the dimensionless equations (Section 2.4), simplifications for the case of small Reynolds number, Capillary number and relaxation length (Sections 2.5 – 2.8), and at the end a summary of the equations needed to establish a numerical method for the simulation of a channel inflow with moving contact lines (Section 2.9).

2.1 The General Formulation

Let us now consider Shikhmurzaev's model in its formulation for a general gas/liquid/solid system. As usual, the model is based on the incompressible Navier–Stokes equations to describe the flow of the liquid bulk,

$$\nabla \cdot \mathbf{u} = 0 \tag{2.1a}$$

$$\rho \left(\frac{\partial \mathbf{u}}{\partial t} + \mathbf{u} \cdot \nabla \mathbf{u} \right) = \nabla \cdot \mathbf{P} \tag{2.1b}$$

$$\mathbf{P} = -p\mathbf{I} + \mu \left(\nabla \mathbf{u} + (\nabla \mathbf{u})^T \right) \tag{2.1c}$$

where $\mathbf{u}$ is the velocity vector of the liquid, ρ is the (constant) density and μ the (constant) viscosity of the liquid, $\mathbf{I}$ is the unit tensor, and $\mathbf{P}$ is the stress tensor in the liquid bulk. All external forces are assumed to be zero.

At the solid surface, we have to apply the following boundary conditions:

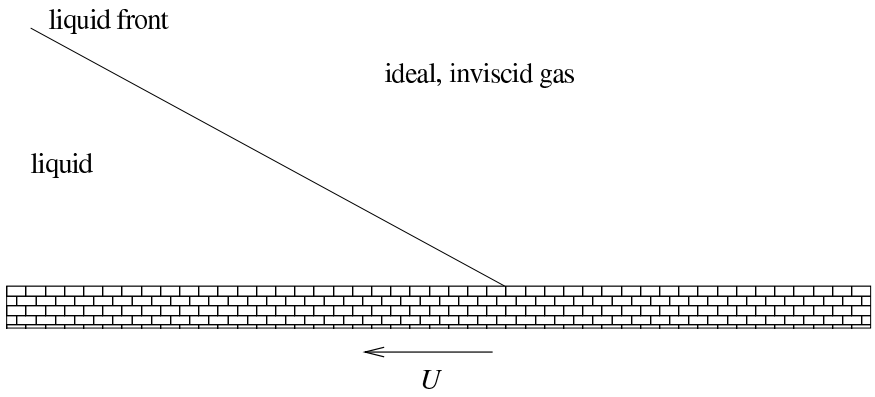

FIGURE 2.1: A solid is moving with speed U along an interface between a liquid and an ideal, inviscid gas

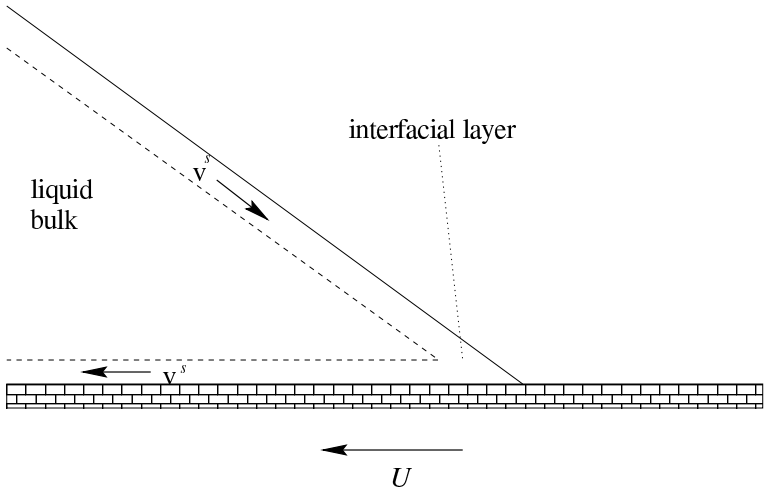

FIGURE 2.2: The interfacial layer adjacent to the boundary

$$p^s = \gamma\,(\rho^s - \rho_0^s) \tag{2.2}$$

where the surface pressure p^s is a pressure forced by intermolecular forces in a thin interfacial layer of the liquid adjacent to the surface (see Figure 2.2). The interfacial layer is assumed to be infinitely thin in this model, and therefore in a three–dimensional flow system p^s is a function of two space variables, and in a two–dimensional flow system p^s is a function of only one space variable. Furthermore, the surface density ρ^s is the corresponding density in that layer, ρ_0^s is the surface density corresponding to zero surface pressure, and γ is a phenomenological coefficient. Equation (2.2) is the surface equation of state in its simplest form: it describes only the dependence of the surface pressure p^s on the surface density ρ^s.

$$\mathbf{n}\cdot\mathbf{P}\cdot(\mathbf{I}-\mathbf{n}\otimes\mathbf{n}) - \frac{1}{2}\nabla p^s = \beta(\mathbf{u}-\mathbf{U})\cdot(\mathbf{I}-\mathbf{n}\otimes\mathbf{n}) \tag{2.3}$$

where $\mathbf{n}$ is an outward normal to the solid surface pointing into the liquid, $\mathbf{n}\cdot\mathbf{P}\cdot(\mathbf{I}-\mathbf{n}\otimes\mathbf{n})$ is the shear stress exerted on the liquid/solid interface by the liquid, β is the coefficient of sliding friction, and $\mathbf{U}$ is the velocity of the solid.

$$\frac{\partial\rho^s}{\partial t} + \nabla\cdot(\rho^s\mathbf{v}^s) = -\frac{\rho^s-\rho_s^s}{\tau} \tag{2.4}$$

where ρ_s^s is the equilibrium surface density at the solid surface, $\mathbf{v}^s$ is the velocity in the liquid layer where p^s and ρ^s exist, and τ is the surface tension relaxation time, i.e. τ characterizes the time interval required for the interfacial structure formation but not for the attatchment of molecules to the solid surface. The right hand side of this equation describes the relaxation of the surface mass density due to the mass exchange between the liquid bulk and the interface. In a flow system with non–singular surface density, we may neglect the mass exchange between the surface and the bulk in the boundary conditions for the bulk flow.

Finally, we must apply some Darcy type equations to relate the surface velocity $\mathbf{v}^s$ with the bulk velocity and the surface pressure gradient,

$$\mathbf{v}^s\cdot(\mathbf{I}-\mathbf{n}\otimes\mathbf{n}) = \frac{1}{2}(\mathbf{u}+\mathbf{U})\cdot(\mathbf{I}-\mathbf{n}\otimes\mathbf{n}) - \alpha\nabla p^s \tag{2.5}$$

$$(\mathbf{v}^s-\mathbf{u})\cdot\mathbf{n} = 0 \tag{2.6}$$

and

$$(\mathbf{v}^s-\mathbf{U})\cdot\mathbf{n} = 0 \tag{2.7}$$

where α is a phenomenological coefficient.

In their general formulation, the boundary conditions at the free liquid surface are the following:

$$p^s = \gamma\,(\rho^s - \rho_0^s) \tag{2.8}$$

which is completely analogous to (2.2).

$$\mathbf{n}\cdot\mathbf{P}\cdot(\mathbf{I}-\mathbf{n}\otimes\mathbf{n}) - \frac{1}{2}\nabla p^s = \beta(\mathbf{u}-\mathbf{u}^{gas})\cdot(\mathbf{I}-\mathbf{n}\otimes\mathbf{n}) \tag{2.9}$$

where $\mathbf{u}^{gas}$ is the velocity of the gas along the liquid front. This equation corresponds to (2.3).

We also have to apply the surface mass balance equation

$$\frac{\partial\rho^s}{\partial t} + \nabla\cdot(\rho^s\mathbf{v}^s) = -\frac{\rho^s-\rho_f^s}{\tau} \tag{2.10}$$

where ρ_f^s denotes the equilibrium surface density at the free surface and $\mathbf{v}^s$ is again the surface velocity.

Furthermore, we need equations at the free surface corresponding to (2.5) – (2.7) at the solid surface. They take the form

$$\mathbf{v}^s\cdot(\mathbf{I}-\mathbf{n}\otimes\mathbf{n}) = \frac{1}{2}(\mathbf{u}+\mathbf{u}^{gas})\cdot(\mathbf{I}-\mathbf{n}\otimes\mathbf{n}) - \alpha\nabla p^s \tag{2.11}$$

$$(\mathbf{v}^s-\mathbf{u})\cdot\mathbf{n} = 0 \tag{2.12}$$

and

$$(\mathbf{v}^s-\mathbf{u}^{gas})\cdot\mathbf{n} = 0 \tag{2.13}$$

In addition to (2.8) – (2.13), we must apply the momentum balance equation for a free surface element,

$$\nabla\cdot\mathbf{P}^s + \mathbf{n}\cdot(\mathbf{P}-\mathbf{P}^{gas}) = \mathbf{0} \tag{2.14}$$

where $\mathbf{P}$ is again the stress tensor in the liquid, $\mathbf{P}^{gas}$ is the stress tensor in the gas, and

$$\mathbf{P}^s = -p^s\,(\mathbf{I} - \mathbf{n} \otimes \mathbf{n}) \tag{2.15}$$

Of course, there is an equation valid at the solid surface which is analogous to (2.14), but we do not need it as a boundary condition there (simply because equations (2.2) – (2.7) are quite enough to describe the behaviour of the flow at the solid boundary).

2.2 Simplification of the Conditions at the Free Liquid Surface

Let us from now on consider the gas to be dynamically passive, i.e. $\mathbf{P}^{gas} = 0$. Thus, equation (2.14) takes the form

$$\nabla \cdot \mathbf{P}^s + \mathbf{n} \cdot \mathbf{P} = \mathbf{0} \tag{2.16}$$

Furthermore, we can rewrite equation (2.11) in the form

$$\mathbf{u}^{gas} \cdot (\mathbf{I} - \mathbf{n} \otimes \mathbf{n}) = (2\mathbf{v}^s - \mathbf{u}) \cdot (\mathbf{I} - \mathbf{n} \otimes \mathbf{n}) + 2\alpha \nabla p^s \tag{2.17}$$

Plugging (2.17) into (2.9), we obtain

$$\mathbf{n} \cdot \mathbf{P} \cdot (\mathbf{I} - \mathbf{n} \otimes \mathbf{n}) - \frac{1}{2}\nabla p^s = 2\beta\,(\mathbf{u} - \mathbf{v}^s) \cdot (\mathbf{I} - \mathbf{n} \otimes \mathbf{n}) - 2\alpha\beta \nabla p^s \tag{2.18}$$

Using (2.16), we can replace equation (2.18) by

$$-\nabla \cdot \mathbf{P}^s \cdot (\mathbf{I} - \mathbf{n} \otimes \mathbf{n}) - \frac{1}{2}\nabla p^s = 2\beta\,(\mathbf{u} - \mathbf{v}^s) \cdot (\mathbf{I} - \mathbf{n} \otimes \mathbf{n}) - 2\alpha\beta \nabla p^s \tag{2.19}$$

From [1], we know that $\mathbf{n} \cdot \mathbf{P}^s = \mathbf{0}$, so $-\nabla \cdot \mathbf{P}^s \cdot (\mathbf{I} - \mathbf{n} \otimes \mathbf{n}) = \nabla p^s$, and thus we can rewrite equation (2.18) as

$$(1 + 4\alpha\beta)\nabla p^s = 4\beta(\mathbf{u} - \mathbf{v}^s) \cdot (\mathbf{I} - \mathbf{n} \otimes \mathbf{n}) \tag{2.20}$$

Let us now examine equation (2.16). Taking its normal projection, we have

$$\begin{aligned} \mathbf{n} \cdot \mathbf{P} \cdot \mathbf{n} &= -\left(\nabla \cdot \mathbf{P}^s\right) \cdot \mathbf{n} \\ &= -\nabla \cdot (\mathbf{P}^s \cdot \mathbf{n}) + \mathbf{P}^s \nabla \cdot \mathbf{n} \\ &= \mathbf{P}^s \nabla \cdot \mathbf{n} \end{aligned} \tag{2.21}$$

because $\mathbf{n} \cdot \mathbf{P}^s = 0$. Thus, we can write

$$\mathbf{n} \cdot \mathbf{P} \cdot \mathbf{n} + p^s \kappa = 0 \tag{2.22}$$

where $\kappa = \nabla \cdot \mathbf{n}$ is the curvature of the free liquid surface.

The tangential projection of (2.16) yields

$$\mathbf{n} \cdot \mathbf{P} \cdot (\mathbf{I} - \mathbf{n} \otimes \mathbf{n}) = -(\nabla \cdot \mathbf{P}^s) \cdot (\mathbf{I} - \mathbf{n} \otimes \mathbf{n}) \tag{2.23}$$

which we can rewrite in the simplified form

$$\mathbf{n} \cdot \mathbf{P} \cdot (\mathbf{I} - \mathbf{n} \otimes \mathbf{n}) - \nabla p^s = 0 \tag{2.24}$$

2.3 Summary of the Model Equations

Summarizing the results from the previous sections, we may formulate the mathematical model for a gas/liquid/solid system in the following way:

- In the liquid bulk, we have the incompressible Navier–Stokes equations

$$\nabla \cdot \mathbf{u} = 0 \tag{2.25a}$$

$$\rho \left(\frac{\partial \mathbf{u}}{\partial t} + \mathbf{u} \cdot \nabla \mathbf{u} \right) = \nabla \cdot \mathbf{P} \tag{2.25b}$$

$$\mathbf{P} = -p\mathbf{I} + \mu \left(\nabla \mathbf{u} + (\nabla \mathbf{u})^T \right) \tag{2.25c}$$

- The conditions at the liquid/solid interface are

$$p^s = \gamma \left(\rho^s - \rho_0^s \right) \tag{2.26}$$

$$\mathbf{n} \cdot \mathbf{P} \cdot (\mathbf{I} - \mathbf{n} \otimes \mathbf{n}) - \frac{1}{2} \nabla p^s = \beta (\mathbf{u} - \mathbf{U}) \cdot (\mathbf{I} - \mathbf{n} \otimes \mathbf{n}) \tag{2.27}$$

$$\frac{\partial \rho^s}{\partial t} + \nabla \cdot (\rho^s \mathbf{v}^s) = -\frac{\rho^s - \rho_s^s}{\tau} \tag{2.28}$$

$$\mathbf{v}^s \cdot (\mathbf{I} - \mathbf{n} \otimes \mathbf{n}) = \frac{1}{2}(\mathbf{u} + \mathbf{U}) \cdot (\mathbf{I} - \mathbf{n} \otimes \mathbf{n}) - \alpha \nabla p^s \tag{2.29}$$

$$(\mathbf{v}^s - \mathbf{u}) \cdot \mathbf{n} = 0 \tag{2.30}$$

$$(\mathbf{v}^s - \mathbf{U}) \cdot \mathbf{n} = 0 \tag{2.31}$$

- The conditions at the liquid/gas interface are

$$p^s = \gamma\,(\rho^s - \rho_0^s) \tag{2.32}$$

$$(1 + 4\alpha\beta)\nabla p^s = 4\beta(\mathbf{u} - \mathbf{v}^s) \cdot (\mathbf{I} - \mathbf{n} \otimes \mathbf{n}) \tag{2.33}$$

$$\frac{\partial \rho^s}{\partial t} + \nabla \cdot (\rho^s \mathbf{v}^s) = -\frac{\rho^s - \rho_f^s}{\tau} \tag{2.34}$$

$$\mathbf{v}^s \cdot (\mathbf{I} - \mathbf{n} \otimes \mathbf{n}) = \frac{1}{2}(\mathbf{u} + \mathbf{u}^{gas}) \cdot (\mathbf{I} - \mathbf{n} \otimes \mathbf{n}) - \alpha \nabla p^s \tag{2.35}$$

$$(\mathbf{v}^s - \mathbf{u}) \cdot \mathbf{n} = 0 \tag{2.36}$$

$$(\mathbf{v}^s - \mathbf{u}^{gas}) \cdot \mathbf{n} = 0 \tag{2.37}$$

$$\mathbf{n} \cdot \mathbf{P} \cdot \mathbf{n} + p^s \kappa = 0 \tag{2.38}$$

$$\mathbf{n} \cdot \mathbf{P} \cdot (\mathbf{I} - \mathbf{n} \otimes \mathbf{n}) - \nabla p^s = 0 \tag{2.39}$$

We will not need conditions (2.35) and (2.37) for the rest of this thesis, and therefore we will ignore them from now on.

2.4 Nondimensionalization

In this section, we want to nondimensionalize the system of equations (2.25) – (2.39). Let us therefore use the following scaling quantities: The characteristic length L, the speed U of the solid wall ($U = |\mathbf{U}|$), the characteristic bulk pressure $\mu U/L$ (this choice will be justified in section 2.5), the equilibrium tension $\sigma = -p^s(\rho_f^s)$ of the free liquid surface, and ρ_0^s, the surface density corresponding to zero surface pressure.

2.4.1 The Navier–Stokes Equations

The incompressible Navier–Stokes equations (2.25) written down in scaled variables take the form

$$\nabla \cdot \mathbf{u} = 0 \tag{2.40a}$$

$$\frac{\rho U^2}{L}\left(\frac{\partial \mathbf{u}}{\partial t} + \mathbf{u}\cdot\nabla\mathbf{u}\right) = \frac{1}{L}\nabla\cdot\mathbf{P} \tag{2.40b}$$

$$\mathbf{P} = \frac{\mu U}{L}\left(-p\mathbf{I} + \nabla\mathbf{u} + (\nabla\mathbf{u})^T\right) \tag{2.40c}$$

Let us now simplify equations (2.40) by plugging (2.40c) into (2.40b). This yields

$$\nabla \cdot \mathbf{u} = 0 \tag{2.41a}$$

$$\frac{\partial \mathbf{u}}{\partial t} + \mathbf{u}\cdot\nabla\mathbf{u} = \frac{\mu}{\rho U L}\nabla\cdot\left(\nabla\mathbf{u} + (\nabla\mathbf{u})^T - p\mathbf{I}\right) \tag{2.41b}$$

Introducing the Reynolds number

$$Re = \frac{\rho U L}{\mu} \tag{2.42}$$

we can now write down the dimensionless, incompressible Navier–Stokes equations in the form

$$\nabla \cdot \mathbf{u} = 0 \tag{2.43a}$$

$$\frac{\partial \mathbf{u}}{\partial t} + \mathbf{u}\cdot\nabla\mathbf{u} = \frac{1}{Re}\nabla\cdot\left(\nabla\mathbf{u} + (\nabla\mathbf{u})^T - p\mathbf{I}\right) \tag{2.43b}$$

In a Cartesian co–ordinate frame (x, y, z), we have $\mathbf{u} = (u, v, w)^T$, and thus

$$\nabla\mathbf{u} = \begin{pmatrix} \frac{\partial u}{\partial x} & \frac{\partial u}{\partial y} & \frac{\partial u}{\partial z} \\ \frac{\partial v}{\partial x} & \frac{\partial v}{\partial y} & \frac{\partial v}{\partial z} \\ \frac{\partial w}{\partial x} & \frac{\partial w}{\partial y} & \frac{\partial w}{\partial z} \end{pmatrix} \tag{2.44}$$

From (2.44) follows

$$\nabla\mathbf{u} + (\nabla\mathbf{u})^T = \begin{pmatrix} 2\frac{\partial u}{\partial x} & \frac{\partial u}{\partial y} + \frac{\partial v}{\partial x} & \frac{\partial u}{\partial z} + \frac{\partial w}{\partial x} \\ \frac{\partial v}{\partial x} + \frac{\partial u}{\partial y} & 2\frac{\partial v}{\partial y} & \frac{\partial v}{\partial z} + \frac{\partial w}{\partial y} \\ \frac{\partial w}{\partial x} + \frac{\partial u}{\partial z} & \frac{\partial w}{\partial y} + \frac{\partial v}{\partial z} & 2\frac{\partial w}{\partial z} \end{pmatrix} \tag{2.45}$$

and therefore we have

$$\begin{aligned}
\nabla\cdot(\nabla\mathbf{u}+(\nabla\mathbf{u})^T) &= \nabla\cdot\begin{pmatrix} 2\frac{\partial u}{\partial x} & \frac{\partial u}{\partial y}+\frac{\partial v}{\partial x} & \frac{\partial u}{\partial z}+\frac{\partial w}{\partial x} \\ \frac{\partial v}{\partial x}+\frac{\partial u}{\partial y} & 2\frac{\partial v}{\partial y} & \frac{\partial v}{\partial z}+\frac{\partial w}{\partial y} \\ \frac{\partial w}{\partial x}+\frac{\partial u}{\partial z} & \frac{\partial w}{\partial y}+\frac{\partial v}{\partial z} & 2\frac{\partial w}{\partial z} \end{pmatrix} \\
&= \begin{pmatrix} 2\frac{\partial^2 u}{\partial x^2}+\frac{\partial^2 u}{\partial y^2}+\frac{\partial^2 v}{\partial x\partial y}+\frac{\partial^2 u}{\partial z^2}+\frac{\partial^2 w}{\partial x\partial z} \\ \frac{\partial^2 v}{\partial x^2}+\frac{\partial^2 u}{\partial x\partial y}+2\frac{\partial^2 v}{\partial y^2}+\frac{\partial^2 v}{\partial z^2}+\frac{\partial^2 w}{\partial y\partial z} \\ \frac{\partial^2 w}{\partial x^2}+\frac{\partial^2 u}{\partial x\partial z}+\frac{\partial^2 w}{\partial y^2}+\frac{\partial^2 v}{\partial y\partial z}+2\frac{\partial^2 w}{\partial z^2} \end{pmatrix} \\
&= \begin{pmatrix} \triangle u+\frac{\partial}{\partial x}(\nabla\cdot\mathbf{u}) \\ \triangle v+\frac{\partial}{\partial y}(\nabla\cdot\mathbf{u}) \\ \triangle w+\frac{\partial}{\partial z}(\nabla\cdot\mathbf{u}) \end{pmatrix} \\
&= \begin{pmatrix} \triangle u \\ \triangle v \\ \triangle w \end{pmatrix} \\
&= \triangle\mathbf{u}
\end{aligned} \tag{2.46}$$

because $\nabla\cdot\mathbf{u}=0$. Furthermore,

$$\nabla\cdot(p\mathbf{I}) = \nabla\cdot\begin{pmatrix} p & 0 & 0 \\ 0 & p & 0 \\ 0 & 0 & p \end{pmatrix} = \begin{pmatrix} \frac{\partial p}{\partial x} \\ \frac{\partial p}{\partial y} \\ \frac{\partial p}{\partial z} \end{pmatrix} = \nabla p \tag{2.47}$$

so that the incompressible Navier–Stokes equations finally take the form

$$\nabla\cdot\mathbf{u}=0 \tag{2.48a}$$

$$\frac{\partial\mathbf{u}}{\partial t}+\mathbf{u}\cdot\nabla\mathbf{u} = \frac{1}{Re}\left(\triangle\mathbf{u}-\nabla p\right) \tag{2.48b}$$

2.4.2 The Conditions at the Solid Surface

Let us nondimensionalize the solid surface equation of state (2.26) using the scaling factors σ for the surface pressure and ρ_0^s for the surface density,

$$p^s = \frac{\gamma\rho_0^s}{\sigma}\left(\rho^s-1\right) \tag{2.49}$$

Defining the parameter

$$\lambda := \frac{\gamma \rho_0^s}{\sigma} \tag{2.50}$$

we can rewrite (2.49) in the form

$$p^s = \lambda \left(\rho^s - 1\right) \tag{2.51}$$

The surface mass balance equation (2.28) written down in dimensionless variables takes the form

$$\frac{\rho_0^s U}{L}\frac{\partial \rho^s}{\partial t} + \frac{\rho_0^s U}{L}\nabla \cdot (\rho^s \mathbf{v}^s) = -\rho_0^s \frac{\rho_s - \rho_s^s}{\tau} \tag{2.52}$$

Multiplying (2.52) with τ/ρ_0^s we obtain

$$\frac{\tau U}{L}\frac{\partial \rho^s}{\partial t} + \frac{\tau U}{L}\nabla \cdot (\rho^s \mathbf{v}^s) = -(\rho_s - \rho_s^s) \tag{2.53}$$

Let us now introduce

$$\epsilon := \frac{\tau U}{L} \tag{2.54}$$

so we can rewrite (2.53) as

$$\epsilon \left(\frac{\partial \rho^s}{\partial t} + \nabla \cdot (\rho^s \mathbf{v}^s)\right) = -(\rho^s - \rho_s^s) \tag{2.55}$$

Equations (2.29),(2.30), and (2.31) in dimensionless form are given by

$$\mathbf{v}^s \cdot (\mathbf{I} - \mathbf{n} \otimes \mathbf{n}) = \frac{1}{2}(\mathbf{u} + \mathbf{U}) \cdot (\mathbf{I} - \mathbf{n} \otimes \mathbf{n}) - \frac{\alpha \sigma}{UL}\nabla p^s \tag{2.56}$$

$$(\mathbf{v}^s - \mathbf{u}) \cdot \mathbf{n} = 0 \tag{2.57}$$

and

$$(\mathbf{v}^s - \mathbf{U}) \cdot \mathbf{n} = 0 \tag{2.58}$$

where because of the definition of the scaling factor U, $\mathbf{U}$ is now a unit vector.

Finally, we can write down the dimensionless form of (2.27) as

$$\frac{\mu U}{L}\mathbf{n}\cdot\mathbf{P}\cdot(\mathbf{I}-\mathbf{n}\otimes\mathbf{n})-\frac{\sigma}{2L}\nabla p^s=U\beta(\mathbf{u}-\mathbf{U})\cdot(\mathbf{I}-\mathbf{n}\otimes\mathbf{n}) \tag{2.59}$$

Multiplying (2.59) with L/σ, we can rewrite it as

$$\frac{\mu U}{\sigma}\mathbf{n}\cdot\mathbf{P}\cdot(\mathbf{I}-\mathbf{n}\otimes\mathbf{n})-\frac{1}{2}\nabla p^s=\frac{UL\beta}{\sigma}(\mathbf{u}-\mathbf{U})\cdot(\mathbf{I}-\mathbf{n}\otimes\mathbf{n}) \tag{2.60}$$

Then, after defining the capillary number

$$Ca:=\frac{\mu U}{\sigma} \tag{2.61}$$

we may write it down as

$$Ca\,\mathbf{n}\cdot\mathbf{P}\cdot(\mathbf{I}-\mathbf{n}\otimes\mathbf{n})-\frac{1}{2}\nabla p^s=\frac{UL\beta}{\sigma}(\mathbf{u}-\mathbf{U})\cdot(\mathbf{I}-\mathbf{n}\otimes\mathbf{n}) \tag{2.62}$$

2.4.3 The Conditions at the Free Surface

The nondimensionalization of the free surface equation of state (2.32) goes straightforward:

$$p^s=\lambda\left(\rho^s-1\right) \tag{2.63}$$

The free surface mass balance equation (2.34) is nondimensionalized completely analogous to the nondimensionalization of the corresponding condition at the solid surface, and this results in

$$\epsilon\left(\frac{\partial\rho^s}{\partial t}+\nabla\cdot(\rho^s\mathbf{v}^s)\right)=-(\rho^s-\rho_f^s) \tag{2.64}$$

The dimensionless form of equation (2.39) is

$$\frac{\mu U}{L}\mathbf{n}\cdot\mathbf{P}\cdot(\mathbf{I}-\mathbf{n}\otimes\mathbf{n})-\sigma\nabla p^s=0 \tag{2.65}$$

Using (2.61), we may rewrite (2.65) as

$$\frac{Ca}{L}\mathbf{n}\cdot\mathbf{P}\cdot(\mathbf{I}-\mathbf{n}\otimes\mathbf{n})-\nabla p^s=0 \tag{2.66}$$

Equation (2.38) becomes

$$\frac{\mu U}{L}\mathbf{n}\cdot\mathbf{P}\cdot\mathbf{n}+\sigma p^s\kappa=0 \tag{2.67}$$

Using again (2.61), we can give (2.67) the form

$$\frac{Ca}{L}\mathbf{n}\cdot\mathbf{P}\cdot\mathbf{n}+p^s\kappa=0 \tag{2.68}$$

Finally, condition (2.33) becomes

$$\sigma(1+4\alpha\beta)\nabla p^s=4UL\beta(\mathbf{u}-\mathbf{v}^s)\cdot(\mathbf{I}-\mathbf{n}\otimes\mathbf{n}) \tag{2.69}$$

and equation (2.36) remains

$$(\mathbf{u}-\mathbf{v}^s)\cdot\mathbf{n}=0 \tag{2.70}$$

2.4.4 Summary of the Dimensionless Equations

Summarizing the results of this section, we gain the dimensionless formulation of the mathematical model for a gas/liquid/solid system. It consists of

- the Navier–Stokes equations

$$\nabla\cdot\mathbf{u}=0 \tag{2.71a}$$

$$\frac{\partial\mathbf{u}}{\partial t}+\mathbf{u}\cdot\nabla\mathbf{u}=\frac{1}{Re}\left(\triangle\mathbf{u}-\nabla p\right) \tag{2.71b}$$

- the conditions at the solid surface

$$p^s=\lambda\left(\rho^s-1\right) \tag{2.72}$$

$$\epsilon\left(\frac{\partial\rho^s}{\partial t}+\nabla\cdot(\rho^s\mathbf{v}^s)\right)=-(\rho^s-\rho_s^s) \tag{2.73}$$

$$\mathbf{v}^s\cdot(\mathbf{I}-\mathbf{n}\otimes\mathbf{n})=\frac{1}{2}(\mathbf{u}+\mathbf{U})\cdot(\mathbf{I}-\mathbf{n}\otimes\mathbf{n})-\frac{\alpha\sigma}{UL}\nabla p^s \tag{2.74}$$

$$(\mathbf{u}-\mathbf{v}^s)\cdot\mathbf{n}=0 \tag{2.75}$$

$$Ca\,\mathbf{n}\cdot\mathbf{P}\cdot(\mathbf{I}-\mathbf{n}\otimes\mathbf{n})-\frac{1}{2}\nabla p^s=\frac{UL\beta}{\sigma}(\mathbf{u}-\mathbf{U})\cdot(\mathbf{I}-\mathbf{n}\otimes\mathbf{n}) \tag{2.76}$$

- and the conditions at the free surface

$$p^s=\lambda\,(\rho^s-1) \tag{2.77}$$

$$\epsilon\left(\frac{\partial\rho^s}{\partial t}+\nabla\cdot(\rho^s\mathbf{v}^s)\right)=-(\rho^s-\rho_f^s) \tag{2.78}$$

$$\frac{Ca}{L}\mathbf{n}\cdot\mathbf{P}\cdot(\mathbf{I}-\mathbf{n}\otimes\mathbf{n})-\nabla p^s=0 \tag{2.79}$$

$$\frac{Ca}{L}\mathbf{n}\cdot\mathbf{P}\cdot\mathbf{n}+p^s\kappa=0 \tag{2.80}$$

$$\sigma(1+4\alpha\beta)\nabla p^s=4UL\beta(\mathbf{u}-\mathbf{v}^s)\cdot(\mathbf{I}-\mathbf{n}\otimes\mathbf{n}) \tag{2.81}$$

$$(\mathbf{u}-\mathbf{v}^s)\cdot\mathbf{n}=0 \tag{2.82}$$

2.5 Steady Flow with $Re, Ca, \epsilon \to 0$

Let us now consider a steady flow where the velocity components parallel to the moving contact line are zero. Steady flow means that the time derivatives in equations (2.71b), (2.73), and (2.78) vanish, while the second assumption justifies the use of a plane co–ordinate frame. Let us further assume that

$$Re \ll 1 \tag{2.83}$$

$$Ca \ll 1 \tag{2.84}$$

and

$$\epsilon \ll 1 \tag{2.85}$$

where (2.85) means that the relaxation length

$$l := U\tau \tag{2.86}$$

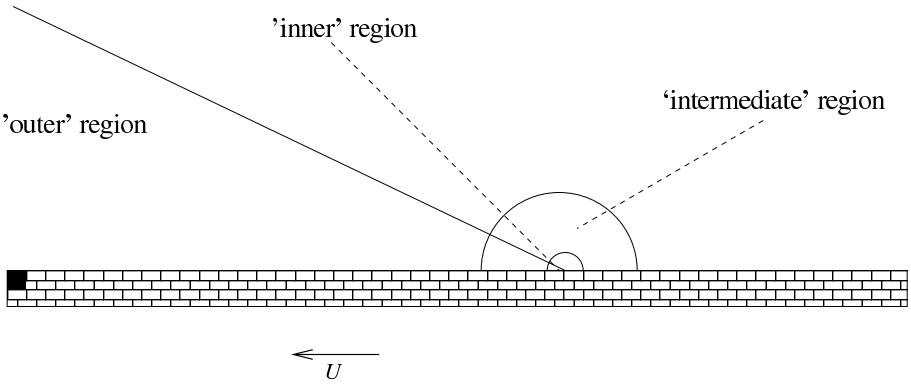

FIGURE 2.3: The asymptotic regions around the contact line

is much smaller than the characteristic length scale L of the flow system (because $\epsilon = l/L$).

Now is the time to justify the choice of the characteristic bulk pressure $\mu U/L$ as scaling quantity for p (see Section 2.4). Plugging (2.42), (2.61), and (2.54) into (2.83), (2.84), and (2.85), respectively, we obtain

$$\frac{\rho U L}{\mu} \ll 1 \tag{2.87}$$

$$\frac{\mu U}{\sigma} \ll 1 \tag{2.88}$$

and

$$\frac{U\tau}{L} \ll 1 \tag{2.89}$$

Due to the fact that the characteristic length scale of a flow system and the density of a liquid must always be finite, inequality (2.87) demands that either $U \ll 1$, or $\mu \gg 1$, or both of them. However, considering the case $\mu \gg 1$, we realize that (2.88) can only hold if $U \ll 1$ and simultaneously $\sigma \gg 1$, and the latter condition is not acceptable from a physical point of view because σ is rather small for any common liquid. Therefore, from (2.87) and (2.88) follows that

$$U \ll 1 \tag{2.90}$$

and

$$\mu = O(1) \tag{2.91}$$

The classical scaling quantity for the pressure is ρU^2 [9, 17], but with finite ρ this quantity is $O(U^2)$ and therefore too small to be used as a scaling quantity. However, we may scale p with the characteristic bulk pressure $\mu U/L$ which is $O(U)$ as long as μ and L are $O(1)$. Therefore, the scaling quantities for velocity and pressure have the same order of magnitude, and the pressure remains in the governing equations for the flow field as $Re, Ca, \epsilon \to 0$. To finish this discussion, let us check the physical dimension of $\mu U/L$:

$$\begin{aligned} \frac{\mu\,[kg/(m\ s)]\,U\,[m/s]}{L\,[m]} &= \frac{\mu U}{L}\left[\frac{kg\ m}{m^2\ s^2}\right] \\ &= \frac{\mu U}{L}\left[\frac{kg}{m\ s^2}\right] \end{aligned} \tag{2.92}$$

which is in fact a pressure.

Due to the fact that the system of equations (2.71) – (2.82) is singularly perturbed as $Ca, \epsilon \to 0$, we may analyze it using the technique of matched asymptotic expansion. Let us therefore establish three asymptotic regions as $Ca, \epsilon \to 0$: the 'outer' region with characteristic length scale L, the 'intermediate' region with characteristic length scale ϵL, and the 'inner' region with characteristic length scale $\epsilon Ca L$ (see Figure 2.3). In other words, in the 'outer' region we neglect all terms of $O(Re)$, $O(Ca)$, and $O(\epsilon)$, in the 'intermediate' region we keep the terms of $O(\epsilon)$, and in the 'inner' region we also keep the terms of $O(Ca)$. Since in the 'inner' and 'intermediate' asymptotic regions a deviation from the classical no–slip boundary condition at the solid boundary takes place, the union of these two is referred to as the slip region.

In the following calculations, we will assume that $Ca \ln \epsilon = o(1)$ as $Ca, \epsilon \to 0$ because this makes the solutions in the 'outer' and slip regions directly matchable [4].

Now we may analyze the above system of equations, and we will do so in a plane polar co–ordinate system (r, θ) whose origin is fixed to the contact line, as shown in Figure 2.4. From now on, angles will always be given in degrees.

2.6 The 'Outer' Region

Neglecting all time derivatives and considering only terms of $O(1)$ as $Re, Ca, \epsilon \to 0$, the system of equations (2.71) – (2.82) reduces to

- the stationary Stokes equations

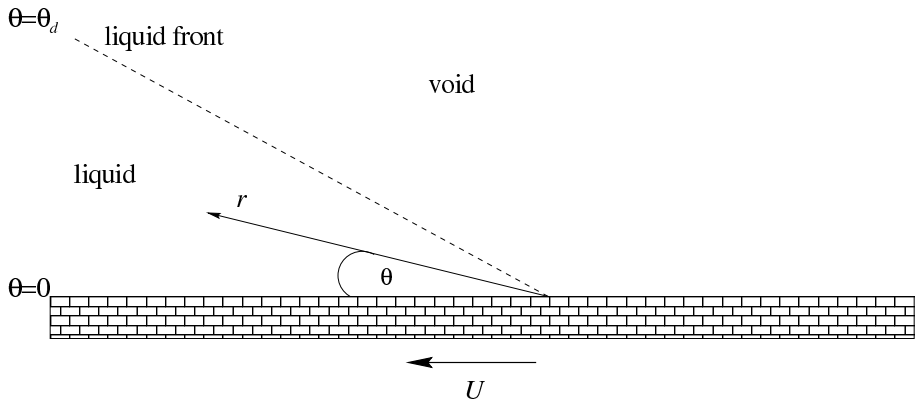

FIGURE 2.4: The co–ordinate frame (r, θ)

$$\nabla \cdot \mathbf{u} = 0 \tag{2.93a}$$

$$\triangle \mathbf{u} = \nabla p \tag{2.93b}$$

- the conditions at the solid surface

$$p^s = \lambda \left(\rho^s - 1 \right) \tag{2.94}$$

$$\rho^s = \rho_s^s \tag{2.95}$$

$$\mathbf{v}^s \cdot (\mathbf{I} - \mathbf{n} \otimes \mathbf{n}) = \frac{1}{2} (\mathbf{u} + \mathbf{U}) \cdot (\mathbf{I} - \mathbf{n} \otimes \mathbf{n}) - \frac{\alpha \sigma}{UL} \nabla p^s \tag{2.96}$$

$$(\mathbf{v}^s - \mathbf{u}) \cdot \mathbf{n} = 0 \tag{2.97}$$

$$(\mathbf{v}^s - \mathbf{U}) \cdot \mathbf{n} = 0 \tag{2.98}$$

$$-\frac{1}{2} \nabla p^s = \frac{UL\beta}{\sigma} (\mathbf{u} - \mathbf{U}) \cdot (\mathbf{I} - \mathbf{n} \otimes \mathbf{n}) \tag{2.99}$$

- and the conditions at the free surface

$$p^s = \lambda \left(\rho^s - 1 \right) \tag{2.100}$$

$$\rho^s = \rho_f^s \tag{2.101}$$

$$\nabla p^s = 0 \tag{2.102}$$

$$p^s \kappa = 0 \tag{2.103}$$

$$\sigma(1 + 4\alpha\beta)\nabla p^s = 4UL\beta(\mathbf{u} - \mathbf{v}^s) \cdot (\mathbf{I} - \mathbf{n} \otimes \mathbf{n}) \tag{2.104}$$

$$(\mathbf{u} - \mathbf{v}^s) \cdot \mathbf{n} = 0 \tag{2.105}$$

Let us first examine the conditions at the solid surface. From (2.95), we get that ρ^s is in equilibrium state and thus constant along the solid surface in the 'outer' region. Plugging this result into (2.94), we obtain that p^s is also constant along the solid surface in the outer region, and thus the surface pressure gradients in (2.96) and (2.99) vanish. From (2.98), we get

$$\mathbf{v}^s \cdot \mathbf{n} = \mathbf{U} \cdot \mathbf{n} \tag{2.106}$$

and putting this result into (2.97) we obtain

$$\mathbf{U} \cdot \mathbf{n} = \mathbf{u} \cdot \mathbf{n} \tag{2.107}$$

Furthermore, from the remainder of (2.99) we get

$$\mathbf{u} \cdot (\mathbf{I} - \mathbf{n} \otimes \mathbf{n}) = \mathbf{U} \cdot (\mathbf{I} - \mathbf{n} \otimes \mathbf{n}) \tag{2.108}$$

Combining (2.107) and (2.108), we obtain the usual no–slip condition

$$\mathbf{u} = \mathbf{U} \tag{2.109}$$

along the solid surface in the 'outer' asymptotic region.

Considering the conditions at the free liquid surface in an analogous way, we obtain from (2.101) that ρ^s is in equilibrium in the 'outer' region and thus $p^s = const$, so again all surface pressure gradients vanish. From (2.103) follows that

$$\kappa = 0 \tag{2.110}$$

which means that we have to deal with a plane liquid front in the 'outer' asymptotic region. Furthermore, combining the remainder of (2.104) with (2.105) we obtain $\mathbf{u} = \mathbf{v}^s$ along the liquid front. In other words,

$$\mathbf{u} = const \tag{2.111}$$

along the free surface in the 'outer' asymptotic region.

Due to (2.110), the two dimensional liquid domain is a wedge shaped region, as drawn in Figures 2.1, 2.3, and 2.4, and thus it is very convenient to solve the problem in a plane spherical co–ordinate frame (r, θ) whose origin coincides with the contact line, as shown in Figure 2.4. In such a coordinate frame, $\mathbf{U}$ has no angular component because it points directly to the direction of the radius vector at $\theta = 0$.

Let us now introduce a stream function $\Psi_{(0)}$, such that

$$u_{r(0)} = \frac{1}{r}\frac{\partial \Psi_{(0)}}{\partial \theta} \tag{2.112a}$$

$$u_{\theta(0)} = -\frac{\partial \Psi_{(0)}}{\partial r} \tag{2.112b}$$

where $u_{r(0)}$ and $u_{\theta(0)}$ are the radial and angular components of the liquid velocity in the 'outer' region, respectively. Using (2.112), we may derive the stream function formulation of the stationary Stokes equations (2.93) in the following way: First, we note that the continuity equation (2.93a) is fulfilled automatically,

$$\begin{aligned} \nabla \cdot \mathbf{u} &= \frac{1}{r}\frac{\partial}{\partial r}(r u_{r(0)}) + \frac{1}{r}\frac{\partial u_{\theta(0)}}{\partial \theta} \\ &= \frac{1}{r}\left(\frac{\partial^2 \Psi_{(0)}}{\partial \theta \partial r} - \frac{\partial^2 \Psi_{(0)}}{\partial r \partial \theta}\right) \\ &= 0 \end{aligned} \tag{2.113}$$

and then we take the curl of (2.93b),

$$\nabla \times \triangle \mathbf{u} = \nabla \times \nabla p \tag{2.114}$$

Due to the fact that the curl of a gradient is always zero, (2.114) reduces to the stationary Stokes equation in stream function formulation:

$$\nabla \times (\triangle \mathbf{u}) = 0 \tag{2.115}$$

$$\Leftrightarrow \triangle (\nabla \times \mathbf{u}) = 0 \tag{2.116}$$

$$\Leftrightarrow \triangle^2 \Psi_{(0)} = 0 \tag{2.117}$$

The no–slip boundary condition (2.109) in stream function formulation becomes

$$\frac{1}{r}\frac{\partial \Psi_{(0)}}{\partial \theta} = U \tag{2.118}$$

$$\frac{\partial \Psi_{(0)}}{\partial r} = 0 \tag{2.119}$$

and

$$\Psi_{(0)} = 0 \tag{2.120}$$

at the solid surface. At the free surface, we have

$$\frac{\partial^2 \Psi_{(0)}}{\partial \theta^2} = 0 \tag{2.121}$$

$$\frac{\partial^2 \Psi_{(0)}}{\partial r^2} = 0 \tag{2.122}$$

and

$$\Psi_{(0)} = 0 \tag{2.123}$$

The solution of (2.117) with boundary conditions (2.118) – (2.120) at the solid surface and (2.121) – (2.123) at the free surface is given by [10]

$$\Psi_{(0)}(r,\theta) = \frac{r}{\sin\theta_d \cos\theta_d - \theta_d}\left[(\theta - \theta_d)\sin\theta - \theta\cos\theta_d \sin(\theta - \theta_d)\right] \tag{2.124}$$

where θ_d denotes the dynamic contact angle of the liquid. We do not yet know θ_d, but later on in this thesis we will derive a formula to compute it directly from the problem parameters.

Please remember that this solution is only valid for gas/liquid/solid systems with a plane liquid front with no additional boundaries or sources of motion close to the moving contact line.

2.7 The Slip Region

2.7.1 The Governing Equations

Let us now continue with the treatment of the 'intermediate' asymptotic region. Please remember that the characteristic length scale of this region was chosen to be $\epsilon L = l = U\tau$, so we have to rescale the system of equations (2.71) – (2.82) by replacing the characteristic length scale L of the 'outer' region with the characteristic length scale l of the 'intermediate' region. Please note that therefore $\epsilon = U\tau/L$ becomes $U\tau/U\tau = 1$. Skipping again all time derivatives and all terms of $O(Ca)$, we obtain

- again the stationary Stokes equations

$$\nabla \cdot \mathbf{u} = 0 \tag{2.125a}$$

$$\triangle \mathbf{u} = \nabla p \tag{2.125b}$$

- the conditions at the solid surface

$$p^s = \lambda(\rho^s - 1) \tag{2.126}$$

$$\nabla \cdot (\rho^s \mathbf{v}^s) = -(\rho^s - \rho_s^s) \tag{2.127}$$

$$\mathbf{v}^s \cdot (\mathbf{I} - \mathbf{n} \otimes \mathbf{n}) = \frac{1}{2}(\mathbf{u} + \mathbf{U}) \cdot (\mathbf{I} - \mathbf{n} \otimes \mathbf{n}) - \frac{\alpha\sigma}{U^2\tau}\nabla p^s \tag{2.128}$$

$$(\mathbf{v}^s - \mathbf{u}) \cdot \mathbf{n} = 0 \tag{2.129}$$

$$(\mathbf{v}^s - \mathbf{U}) \cdot \mathbf{n} = 0 \tag{2.130}$$

$$-\frac{1}{2}\nabla p^s = \frac{U^2\tau\beta}{\sigma}(\mathbf{u} - \mathbf{U}) \cdot (\mathbf{I} - \mathbf{n} \otimes \mathbf{n}) \tag{2.131}$$

- and the conditions at the free surface

$$p^s = \lambda(\rho^s - 1) \tag{2.132}$$

$$\nabla \cdot (\rho^s \mathbf{v}^s) = -(\rho^s - \rho_f^s) \tag{2.133}$$

$$\nabla p^s = 0 \tag{2.134}$$

$$p^s \kappa = 0 \tag{2.135}$$

$$\sigma(1 + 4\alpha\beta)\nabla p^s = 4U^2 \tau\beta(\mathbf{u} - \mathbf{v}^s) \cdot (\mathbf{I} - \mathbf{n} \otimes \mathbf{n}) \tag{2.136}$$

$$(\mathbf{u} - \mathbf{v}^s) \cdot \mathbf{n} = 0 \tag{2.137}$$

Please note that due to equation (2.135), we have again a plane liquid front and thus a wedge shaped liquid domain, as drawn in Figures 2.1, 2.3, and 2.4. In such a liquid domain, the radius vector is always tangential to a given liquid surface, and the angular direction is always normal to a given liquid surface, so we have along the surfaces of the liquid domain

$$\mathbf{v}^s \cdot (\mathbf{I} - \mathbf{n} \otimes \mathbf{n}) = v_r^s \tag{2.138}$$

$$\mathbf{v}^s \cdot \mathbf{n} = v_\theta^s \tag{2.139}$$

where v_r^s and v_θ^s are the radial and angular component of $\mathbf{v}^s$ along the corresponding liquid surface, respectively,

$$\mathbf{u} \cdot (\mathbf{I} - \mathbf{n} \otimes \mathbf{n}) = u_r(r, \theta) \tag{2.140}$$

$$\mathbf{u} \cdot \mathbf{n} = u_\theta(r, \theta) \tag{2.141}$$

where u_r and u_θ are the radial and angular component of $\mathbf{u}$, respectively, $\theta = 0$ along the solid boundary, and $\theta = \theta_d$ along the free boundary of the liquid domain,

$$\mathbf{U} \cdot (\mathbf{I} - \mathbf{n} \otimes \mathbf{n}) = 1 \tag{2.142}$$

$$\mathbf{U} \cdot \mathbf{n} = 0 \tag{2.143}$$

because $\mathbf{U}$ is a unit vector in radial direction along the liquid/solid interface ($U = |\mathbf{U}|$ is the characteristic speed of the flow system), and

$$\nabla p^s = \frac{\mathrm{d}}{\mathrm{d}r} p^s \tag{2.144}$$

since in a plane co–ordinate frame p^s depends only on one space variable, and due to the fact that both boundaries of the liquid domain are straight lines, this one space variable is always the radial co–ordinate.

We may now eliminate the surface pressure p^s from all boundary conditions by applying (2.126) at the solid boundary and (2.132) at the free boundary. Applying also (2.138) – (2.144), we can rewrite the conditions at the solid surface. Thus, equation (2.128) yields

$$v_r^s = \frac{1}{2}(u_r(r,0)+1) - \frac{\alpha\gamma\rho_0^s}{U^2\tau}\frac{\mathrm{d}}{\mathrm{d}r}\rho^s \tag{2.145}$$

Solving (2.145) for $u_r(r,0)$ we get

$$u_r(r,0) = 2v_r^s - 1 + \frac{2\alpha\gamma\rho_0^s}{U^2\tau}\frac{\mathrm{d}}{\mathrm{d}r}\rho^s \tag{2.146}$$

Let us now expand the fraction on the right hand side of equation (2.146) by $\beta(1+4\alpha\beta)$, which yields

$$\frac{2\alpha\gamma\rho_0^s}{U^2\tau}\beta = \frac{2\alpha\beta\gamma\rho_0^s(1+4\alpha\beta)}{U^2\tau\beta(1+4\alpha\beta)} \tag{2.147}$$

Introducing the parameters

$$A := \alpha\beta \tag{2.148}$$

and

$$V := U\sqrt{\frac{\tau\beta}{\sigma\lambda(1+4A)}} \tag{2.149}$$

and using (2.50), we may rewrite (2.147) as

$$\frac{2\alpha\gamma\rho_0^s}{U^2\tau}\beta = \frac{2A}{(1+4A)V^2} \tag{2.150}$$

Finally applying (2.150) to equation (2.146) we obtain

$$u_r(r,0) = 2v_r^s - 1 + \frac{2A}{(1+4A)V^2}\frac{\mathrm{d}}{\mathrm{d}r}\rho^s \tag{2.151}$$

Solving (2.130) for $\mathbf{v}^s \cdot \mathbf{n}$, putting the result into (2.129) and applying (2.141) and (2.143) we obtain

$$u_\theta(r,0) = 0 \tag{2.152}$$

and substituting (2.139), (2.141), and (2.152) into equation (2.129), we get

$$v_\theta^s = 0 \tag{2.153}$$

From (2.153) we obtain

$$\nabla \cdot (\rho^s \mathbf{v}^s) = \nabla \cdot (\rho^s v_r^s) = \frac{\mathrm{d}}{\mathrm{d}r}(\rho^s v_r^s) \tag{2.154}$$

and therefore equation (2.127) simplifies to

$$\frac{\mathrm{d}}{\mathrm{d}r}(\rho^s v_r^s) = -(\rho^s - \rho_s^s) \tag{2.155}$$

Remark: It is also possible to justify (2.154) heuristically by claiming that $\mathbf{v}^s$ and ρ^s do only exist in the interfacial liquid layer along the boundary, and therefore they depend only on r and not on θ; furthermore, the radial component of $\mathbf{v}^s$ must be equal to zero. Therefore, analogous to (2.144), one obtains (2.154).

Applying (2.126),(2.140),(2.142), and (2.144) to equation (2.131), we obtain

$$-\frac{1}{2}\lambda \frac{\mathrm{d}}{\mathrm{d}r}\rho^s = \frac{U^2\tau\beta}{\sigma}(u_r(r,0) - 1) \tag{2.156}$$

Let us now put (2.151) into (2.156). This results in

$$-\frac{1}{2}\lambda \frac{\mathrm{d}}{\mathrm{d}r}\rho^s = \frac{U^2\tau\beta}{\sigma}(2v_r^s - 1 + \frac{2A}{(1+4A)V^2}\frac{\mathrm{d}}{\mathrm{d}r}\rho^s - 1) \tag{2.157}$$

Rewriting (2.157), we obtain

$$-\frac{\mathrm{d}}{\mathrm{d}r}\rho^s = 4\frac{U^2\sigma\lambda}{\gamma\rho_0^s}(v_r^s - 1) + 4\frac{U^2\tau\beta}{\sigma\lambda}\frac{A}{(1+4A)V^2}\frac{\mathrm{d}}{\mathrm{d}r}\rho^s \tag{2.158}$$

and using (2.149) yields

$$-\frac{\mathrm{d}}{\mathrm{d}r}\rho^s = 4\frac{U^2\tau\beta}{\gamma\rho_0^s}(v_r^s - 1) + 4A\frac{\mathrm{d}}{\mathrm{d}r}\rho^s \tag{2.159}$$

Using again (2.149), equation (2.159) can be rewritten in the more simple form

$$-\frac{\mathrm{d}}{\mathrm{d}r}\rho^s = 4V^2(v_r^s - 1) \tag{2.160}$$

Now we want to treat the conditions at the free boundary in a similar way. Applying (2.144) and (2.132) to equation (2.134), we get

$$\frac{\mathrm{d}}{\mathrm{d}r}\rho^s = 0 \tag{2.161}$$

We may obtain a second condition for the free liquid surface by combining (2.132), (2.136), (2.144), (2.148), and (2.149), namely

$$\frac{\mathrm{d}}{\mathrm{d}r}\rho^s = 4V^2(u_r(r,\theta_d) - v_r^s) \tag{2.162}$$

Combining (2.137), (2.139), and (2.141), we get

$$u_\theta(r,\theta_d) = v_\theta^s \tag{2.163}$$

Due to the fact that the liquid front is constrained to be plane, v_θ^s can only vary as long as θ_d varies. But for physical reasons θ_d is always constant in stationary flow, so we have

$$v_\theta^s = 0 \tag{2.164}$$

and therefore

$$u_\theta(r,\theta_d) = 0 \tag{2.165}$$

Finally applying (2.164) to equation (2.133), we obtain completely analogously to the derivation of (2.155)

$$\frac{\mathrm{d}}{\mathrm{d}r}(\rho^s v_r^s) = -(\rho^s - \rho_f^s) \tag{2.166}$$

In the 'inner' asymptotic region, the characteristic length scale was chosen to be $Ca\epsilon L$. Since we consider only terms of $O(1)$ as $Ca \to 0$, the characteristic length scale and thus the dimensions of the 'inner' asymptotic region can be neglected. Therefore, the slip region of the flow system considered here consists only of the 'intermediate' asymptotic region.

2.7.2 The Boundary Conditions for the Slip Region

Summarizing the results of subsection (2.7.1), we have

- at the solid boundary of the slip region

$$\frac{\mathrm{d}}{\mathrm{d}r}(\rho^s v_r^s) = -(\rho^s - \rho_s^s) \tag{2.167}$$

$$u_r(r,0) = 2v_r^s - 1 + \frac{2A}{(1+4A)V^2}\frac{\mathrm{d}}{\mathrm{d}r}\rho^s \tag{2.168}$$

$$u_\theta(r,0) = 0 \tag{2.169}$$

$$-\frac{\mathrm{d}}{\mathrm{d}r}\rho^s = 4V^2(v_r^s - 1) \tag{2.170}$$

- and at the free boundary of the slip region

$$\frac{\mathrm{d}}{\mathrm{d}r}(\rho^s v_r^s) = -(\rho^s - \rho_f^s) \tag{2.171}$$

$$\frac{\mathrm{d}}{\mathrm{d}r}\rho^s = 0 \tag{2.172}$$

$$\frac{\mathrm{d}}{\mathrm{d}r}\rho^s = 4V^2(u_r(r,\theta_d) - v_r^s) \tag{2.173}$$

$$u_\theta(r,\theta_d) = 0 \tag{2.174}$$

We must match the solutions in the 'outer' region and the slip region, so we have the additional conditions

- at the solid surface

$$\lim_{r\to\infty} \rho^s = \rho_s^s \tag{2.175}$$

$$\lim_{r\to\infty} u(r,0) = 1 \tag{2.176}$$

- and at the free surface

$$\lim_{r\to\infty} \rho^s = \rho_f^s \tag{2.177}$$

$$\lim_{r\to\infty} u(r,0) = u_{r(0)}(\theta_d) \tag{2.178}$$

We can easily compute $u_{r(0)}(\theta_d)$ by applying (2.112a) to (2.124) and letting $\theta = \theta_d$ in the result. This yields

$$u_{r(0)}(\theta_d) = \frac{\sin\theta_d - \theta_d\cos\theta_d}{\sin\theta_d\cos\theta_d - \theta_d} \tag{2.179}$$

Furthermore, we have the mass balance equation at the moving contact line,

$$\rho^s v_r^s|_{r\to 0,\theta=\theta_d} + \rho^s v_r^s|_{r\to 0,\theta=0} = 0 \tag{2.180}$$

and the Young equation governing the force balance at the moving contact line,

$$p^s|_{r\to 0,\theta=\theta_d}\cos\theta_d = p_S^s - p^s|_{r\to 0,\theta=0} \tag{2.181}$$

where p_S^s is the reacting force component acting on the contact line element tangential to the solid surface from the solid.

Let us now integrate the conditions at the free liquid surface. From (2.172) and (2.177), we obtain

$$\rho^s = \rho_f^s \tag{2.182}$$

Plugging (2.182) into equation (2.173) yields

$$v_r^s = u_r(r,\theta_d) \tag{2.183}$$

and finally putting (2.182) and (2.183) into equation (2.171) and applying (2.178) gives

$$u_r(r,\theta_d) = u_{r(0)}(\theta_d) \tag{2.184}$$

The treatment of the solid boundary is much more complicated. Here, we rely on the fact that for most liquids the parameter λ is much greater than unity [13].

Therefore, we may consider $1/\lambda$ as a small parameter and expand ρ^s and u_r^s asymptotically in $1/\lambda$,

$$\rho^s = \rho_s^s + \frac{1}{\lambda}\rho_1^s + O\left(\frac{1}{\lambda^2}\right) \tag{2.185}$$

$$v_r^s = 1 + \frac{1}{\lambda}v_{r,1}^s + O\left(\frac{1}{\lambda^2}\right) \tag{2.186}$$

Putting (2.185) and (2.186) into equation (2.170), we obtain

$$v_{r,1}^s = -\frac{1}{4V^2}\frac{\mathrm{d}}{\mathrm{d}r}\rho_1^s \tag{2.187}$$

Let us now plug (2.185) and (2.186) into equation (2.167) and collect all terms of $O(1/\lambda)$. This yields

$$\rho_s^s \frac{\mathrm{d}}{\mathrm{d}r}v_{r,1}^s + \frac{\mathrm{d}}{\mathrm{d}r}\rho_1^s = \rho_1^s \tag{2.188}$$

Combining (2.187) and (2.188) results in

$$-\frac{\rho_s^s}{4V^2}\frac{\mathrm{d}^2}{\mathrm{d}r^2}\rho_1^s + \frac{\mathrm{d}}{\mathrm{d}r}\rho_1^s = \rho_1^s \tag{2.189}$$

The general solution of (2.189) is

$$\rho_1^s = B\exp\left(\frac{2V}{\rho_s^s}\left(V - \sqrt{V^2+\rho_s^s}\right)r\right) + C\exp\left(\frac{2V}{\rho_s^s}\left(V + \sqrt{V^2+\rho_s^s}\right)r\right) \tag{2.190}$$

where B and C are the constants of integration. Condition (2.175) together with (2.185) gives

$$\lim_{r\to\infty}\rho_1^s = 0 \tag{2.191}$$

so that C must be equal to zero, and we can rewrite (2.190) as

$$\rho_1^s = B\exp(-qr) \tag{2.192}$$

where

$$q = \frac{2V}{\rho_s^s}\left(\sqrt{V^2+\rho_s^s} - V\right) \tag{2.193}$$

and (2.185) becomes

$$\rho^s = \rho_s^s + \frac{B}{\lambda}\exp(-qr) + O\left(\frac{1}{\lambda^2}\right) \tag{2.194}$$

Now we can compute $v_{r,1}^s$ by plugging (2.192) into equation (2.187). This results in

$$v_{r,1}^s = \frac{qB}{4V^2}\exp(-qr) \tag{2.195}$$

and therefore we have

$$v_r^s = 1 + \frac{qB}{4\lambda V^2}\exp(-qr) + O\left(\frac{1}{\lambda^2}\right) \tag{2.196}$$

Finally, we may put (2.194) and (2.196) into equation (2.168). This yields

$$\begin{aligned} u_r(r,0) = 2\left(1 + \frac{qB}{4\lambda V^2}\exp(-qr) + O\left(\frac{1}{\lambda^2}\right)\right) - 1 \\ + \frac{2A}{(1+4A)V^2}\frac{\mathrm{d}}{\mathrm{d}r}\left(\rho_s^s + \frac{B}{\lambda}\exp(-qr) + O\left(\frac{1}{\lambda^2}\right)\right) \end{aligned} \tag{2.197}$$

or in simplified form

$$u_r(r,0) = 1 + \frac{(1-\rho_f^s)qB}{2V^2(1+4A)}\exp(-qr) + O\left(\frac{1}{\lambda^2}\right) \tag{2.198}$$

2.7.3 The Constant of Integration

We still do not know the value of the constant of integration B. In order to estimate it, we may now put (2.194) and (2.196) into the momentum balance equation (2.180). This yields

$$\rho^s v_r^s|_{r\to 0,\theta\to\theta_d} + \left(\rho_s^s + \frac{B}{\lambda}\right)\left(1 + \frac{qB}{4\lambda V^2}\right) + O\left(\frac{1}{\lambda^2}\right) = 0 \tag{2.199}$$

which we can rewrite using (2.182) and (2.183) to achieve

$$\rho_f^s u_{r(0)}(\theta_d) + \rho_s^s + \frac{B}{\lambda} + \frac{\rho_s^s qB}{4\lambda V^2} + O\left(\frac{1}{\lambda^2}\right) = 0 \tag{2.200}$$

Now we want to perform a detailed examination of the Young equation (2.181). Let us therefore first express the limiting values of the surface pressure in terms of the surface equations of state (2.126) and (2.132),

$$\lambda(\rho^s - 1)|_{r\to 0,\theta=\theta_d} \cos\theta_d = p_S^s - \lambda(\rho^s - 1)|_{r\to 0,\theta=0} \tag{2.201}$$

Applying (2.182) to equation (2.201), we get

$$\lambda(\rho_f^s - 1)|_{r\to 0,\theta=\theta_d} \cos\theta_d = p_S^s - \lambda(\rho^s - 1)|_{r\to 0,\theta=0} \tag{2.202}$$

Please remember that the scaling quantity for the surface pressure is $\sigma = -p^s(\rho_f^s)$, so we have in dimensionless formulation

$$\lambda(\rho_f^s - 1) = -1 \tag{2.203}$$

and thus we can rewrite equation (2.202) in the form

$$\cos\theta_d = \lambda(\rho^s - 1)|_{r\to 0,\theta=0} - p_S^s \tag{2.204}$$

In the static case, the Young equation (2.204) becomes

$$\cos\theta_s = \lambda(\rho_s^s - 1) - p_S^s \tag{2.205}$$

Let us now rewrite (2.205) as

$$\rho_s^s = 1 + \frac{1}{\lambda}(\cos\theta_s + p_S^s) \tag{2.206}$$

and put (2.206) into (2.200). This results in

$$\rho_f^s u_{r(0)}(\theta_d) + \rho_s^s + \frac{B}{\lambda} + \frac{qB}{4\lambda V^2} + O\left(\frac{1}{\lambda^2}\right) = 0 \tag{2.207}$$

Neglecting the terms of $O(1/\lambda^2)$, we get from (2.207)

$$B = -\lambda\left(\rho_s^s + \rho_f^s u_{r(0)}(\theta_d)\right)\left(\frac{q}{4V^2} + 1\right)^{-1} \tag{2.208}$$

2.8 The Dynamic Contact Angle

Using the results of Section 2.7, we are now able to derive a formula for the computation of the dynamic contact angle θ_d. Let us start with rewriting the static Young equation (2.205) as

$$p_S^s = \lambda(\rho_s^s - 1) - \cos\theta_s \tag{2.209}$$

After this, we put (2.209) into the Young equation for the dynamic case (2.204) to get rid of p_s^s and rewrite the result with both angular terms on the left hand side, so we end up with

$$\cos\theta_s - \cos\theta_d = \lambda(\rho_s^s - 1) - \lambda(\rho^s - 1)|_{r\to 0,\theta\to 0} \tag{2.210}$$

Now we can eliminate ρ^s by using (2.194) with $r \to 0$, so we obtain from (2.210) under neglection of all terms of $O(1/\lambda^s)$

$$\begin{aligned} \cos\theta_s - \cos\theta_d &= \lambda\left(\rho_s^s - 1 - \rho_s^s - \frac{B}{\lambda} + 1\right) \\ &= -B \end{aligned} \tag{2.211}$$

After putting (2.208) into equation (2.211), we can write down the formula for θ_d in its final form,

$$\cos\theta_s - \cos\theta_d = \lambda\left(\rho_s^s + \rho_f^s u_{r(0)}(\theta_d)\right)\left(\frac{q}{4V^2} + 1\right)^{-1} \tag{2.212}$$

2.9 Summary of the Results

Let us now give an overview of the work done so far by summarizing the results of this chapter.

In any asymptotic region, the flow in the liquid bulk is governed by the stationary Stokes equations

$$\nabla \cdot \mathbf{u} = 0 \tag{2.213a}$$

$$\triangle \mathbf{u} = \nabla p \tag{2.213b}$$

In the 'outer' asymptotic region, we have the classical no–slip boundary conditions

$$u_r(r,0) = 1 \tag{2.214}$$

and

$$u_\theta(r,0) = 0 \tag{2.215}$$

at the solid boundary, while the conditions at the free boundary are given by

$$u_r(r,\theta_d) = \frac{\sin\theta_d - \theta_d\cos\theta_d}{\sin\theta_d\cos\theta_d - \theta_d} \tag{2.216}$$

and

$$u_\theta(r,\theta_d) = 0 \tag{2.217}$$

The boundary conditions in the slip region are

$$u_r(r,0) = 1 + \frac{qB}{2\lambda V^2(1+4A)}\exp(-qr) + O\left(\frac{1}{\lambda^2}\right) \tag{2.218}$$

and

$$u_\theta(r,0) = 0 \tag{2.219}$$

at the solid surface as well as

$$u_r(r,\theta_d) = \frac{\sin\theta_d - \theta_d\cos\theta_d}{\sin\theta_d\cos\theta_d - \theta_d} \tag{2.220}$$

and

$$u_\theta(r,\theta_d) = 0 \tag{2.221}$$

at the free surface.

The constants are determined by

$$A = \alpha\beta \tag{2.222}$$

$$V = U\sqrt{\frac{\tau\beta}{\sigma\lambda(1+4A)}} \tag{2.223}$$

$$q = \frac{2V}{\rho_s^s}\left(\sqrt{V^2+\rho_s^s} - V\right) \tag{2.224}$$

$$B = -\lambda\left(\rho_s^s + \rho_f^s u_{r(0)}(\theta_d)\right)\left(\frac{q}{4V^2}+1\right)^{-1} \tag{2.225}$$

and

$$\theta_d = \arccos\left(\cos\theta_s - \lambda\left(\rho_s^s + \rho_f^s u_{r(0)}(\theta_d)\right)\left(\frac{q}{4V^2}+1\right)^{-1}\right) \tag{2.226}$$

Furthermore, we obtain from (2.203) that

$$\lambda = \frac{1}{1-\rho_f^s} \tag{2.227}$$

so we can eliminate λ from all equations given in this section, as well as we can eliminate ρ_s^s in terms of the Young equation for the static case,

$$\rho_s^s = 1 + \frac{1}{\lambda}(\cos\theta_s + p_S^s) \tag{2.228}$$

The equations given in this section are the basis of the numerical method we want to establish in the next chapter.

Chapter 3

The Numerical Method

The numerical method presented in this chapter is based on the Navier–Stokes code NaSt2D by Griebel, Dornseifer and Neunhoeffer [6, 7]. To simulate a channel inflow with moving contact lines, we have to implement the mathematical model given in Chapter 2 into the existing code. We want to restrict ourselfs to steady flow with $Re, Ca, \epsilon \to 0$, so we may apply the model equations as given in Section (2.9).

We will start with some remarks about the mergence of this mathematical model into the existing code (Section 3.1) and the description of the computational grid (Section 3.2), then continue with the numerical treatment of the Stokes equations (Section 3.3) and the free liquid surface (Section 3.4), afterwards we will discuss the boundary conditions to be posed for the flow field (Section 3.5), and finally we will consider the basic features of the problem solver (Section 3.6).

3.1 On the Implementation of the Model into the Existing Code

The main task of this thesis is to give a numerical method for the simulation of a channel inflow, so we have to implement the model equations from Section 2.9 into the already existing code for the simulation of classical fluid flow problems. The main difference between a channel inflow and the situation described in Chapter 2 (the classical void/liquid/solid system) is that we do no longer deal with a wedge shaped liquid domain between a liquid and a gas but with a flow system as shown in Figure 3.1: two parallel solids are moving with the same velocity (a detailed explanation for this will be given in the next paragraph), and between them we have a liquid domain and a void domain. Thus, we have a curved liquid front and two moving contact lines, one at the intersection of each solid with the free liquid surface. We have to establish an 'intermediate' asymptotic region around each moving contact line, as shown in Figure 3.2. The mathematical model we want to

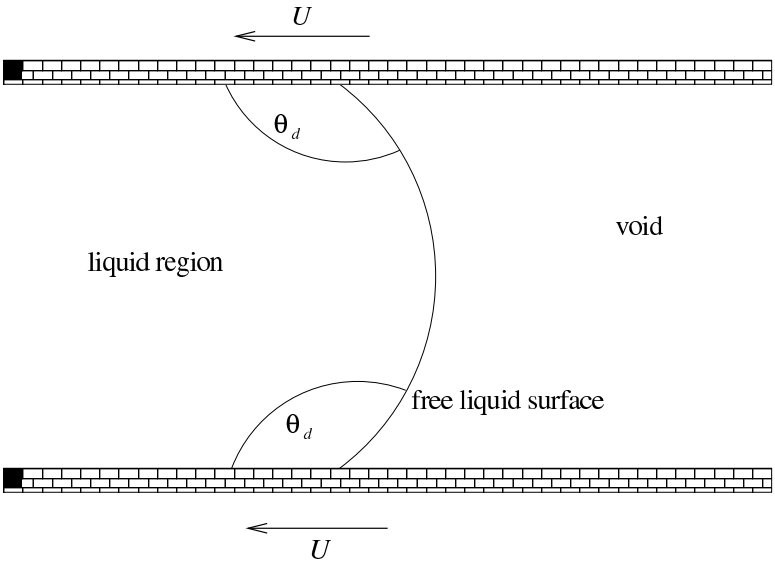

FIGURE 3.1: Channel flow with two moving contact lines

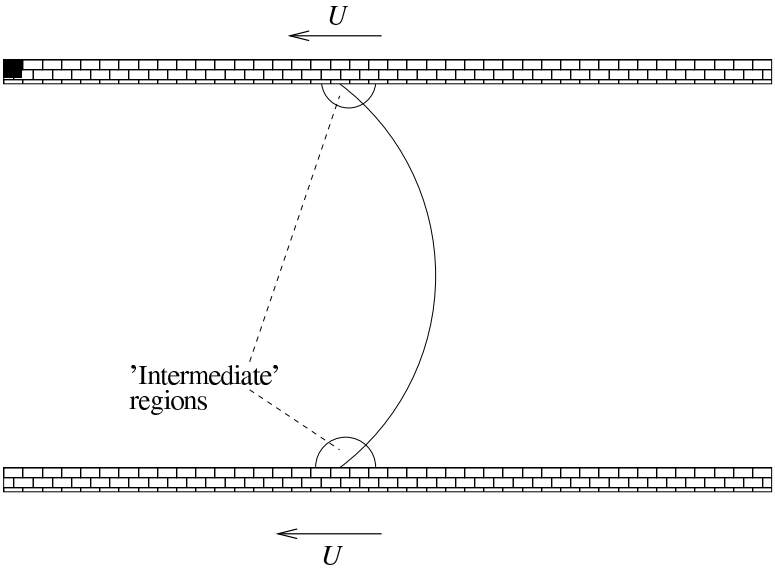

FIGURE 3.2: The asymptotic regions inside the channel

use to simulate the flow in the slip regions is based on the assumption that there is only one solid surface influencing the liquid domain, and therefore we have to take care that the slip regions are small enough that they do not suffer any influence from the solid at the opposite side. In the 'outer' asymptotic region, it is no problem to compute a proper solution with a classical mathematical model for Stokes flow. Furthermore, it is very easy to find a characteristic length for a channel inflow system: we choose L to be equal to the diameter of the channel (which is typical for classical channel flow simulations).

It is convenient to use a co–ordinate frame (and thus a computational grid) fixed with respect to the moving contact line. This implies that the contact line does not move relatively to the grid, and therefore the liquid front remains constant with respect to the computational domain. From a physical point of view, the walls of the channel are of course fixed, the liquid front is moving relatively to the channel, and so is the computational domain. However, from a computational point of view, the liquid front is fixed, and the walls of the channel are moving with constant velocity relatively to the contact lines, see again Figure 3.1.

Another important thing to be done is the transformation of the co–ordinate frame: the mathematical model is given in plane polar co–ordinates (r, θ), while the numerical method is based on plane Cartesian co–ordinates (x, y). Thus, we have to transform the co–ordinates by applying the formulae

$$\mathbf{e}_r = \begin{pmatrix} \cos\theta \\ \sin\theta \end{pmatrix} \quad \text{and} \quad \mathbf{e}_\theta = \begin{pmatrix} -\sin\theta \\ \cos\theta \end{pmatrix} \tag{3.1}$$

where $\mathbf{e}_r$ and $\mathbf{e}_\theta$ are the unit vectors in r and θ direction,respectively, expressed in Cartesian co–ordinates. Applying (3.1) to the quantities given in polar co–ordinates in Section 2.9, we are able to express all of them in Cartesian co–ordinates.

3.2 The Computational Grid

We want to use a Cartesian co–ordinate system (x, y) whose origin is in the lower left corner of the channel extract we want to consider, see Figure 3.3. (Please remember that the co–ordinate frame is fixed with respect to the moving contact line, and so the channel extract we want to consider is physically moving with the contact line, even though it is in rest relative to the chosen co–ordinate system.) Therefore, this channel extract coincides with a rectangle $\Omega \subset \mathbb{R}^2$, where $\Omega := [0, a] \times [0, b]$, a is the domain length in x direction, and b is the domain length in y direction. Let us now cover Ω with an equidistant Cartesian

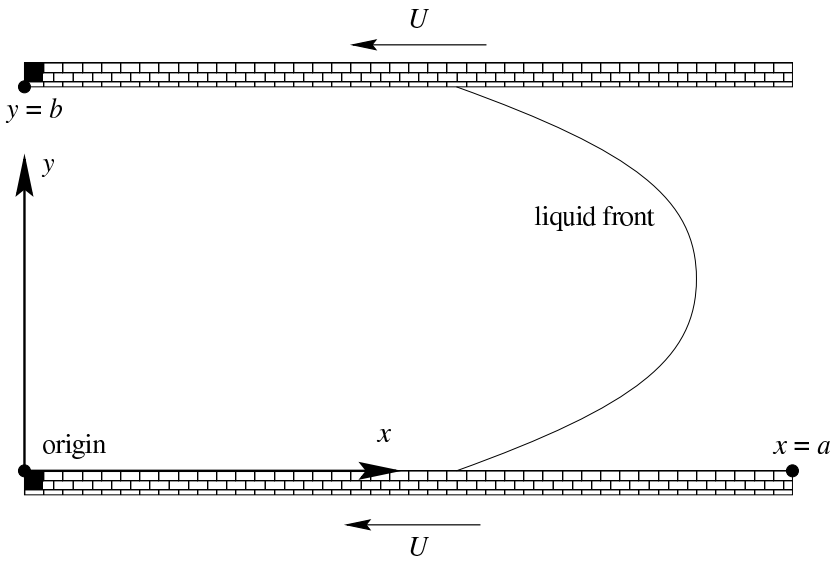

FIGURE 3.3: The co–ordinate system used for the numerical method presented in this chapter

grid which contains i_{max} cells in x direction and j_{max} cells in y direction, such that the distances between the grid lines are

$$\delta x := \frac{a}{i_{max}} \quad \text{and} \quad \delta y := \frac{b}{j_{max}} \tag{3.2}$$

Furthermore, we will use a staggered grid, i.e. we will consider the pressure p at the cell center, the horizontal velocity u at the mid points of the vertical grid lines, and the vertical velocity v at the mid points of the horizontal grid lines, as shown in Figure 3.4. Thus, cell (i, j) covers exactly the region $[(i-1)\delta x, i\delta x] \times [(j-1)\delta y, j\delta y]$, and the index (i, j) denotes p at the center of the cell, u at the grid line right of the cell, and v at the grid line on top of the cell.

In order to make all boundary conditions applicable exactly at the boundaries, we must establish a ghost layer of cells around the domain Ω (see Figure 3.5), such that we can calculate boundary values by linear extrapolation [7] if we do not consider a quantity directly at a given boundary. We will have a detailed discussion of the treatment of the boundary conditions in Section 3.5

3.3 The Treatment of the Stokes Equations

Let us now have a look at the numerical treatment of the stationary Stokes equations,

$$\nabla \cdot \mathbf{u} = 0 \tag{3.3a}$$

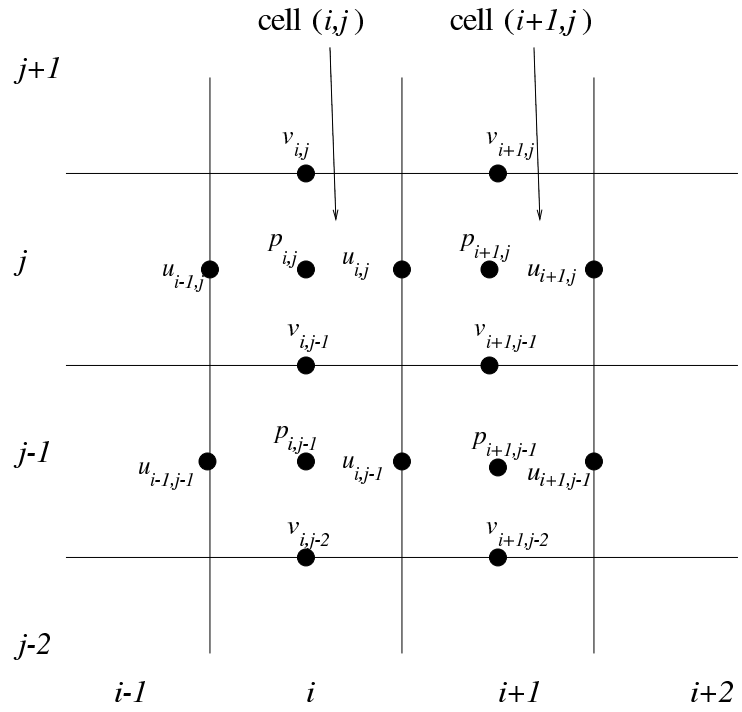

FIGURE 3.4: The staggered grid

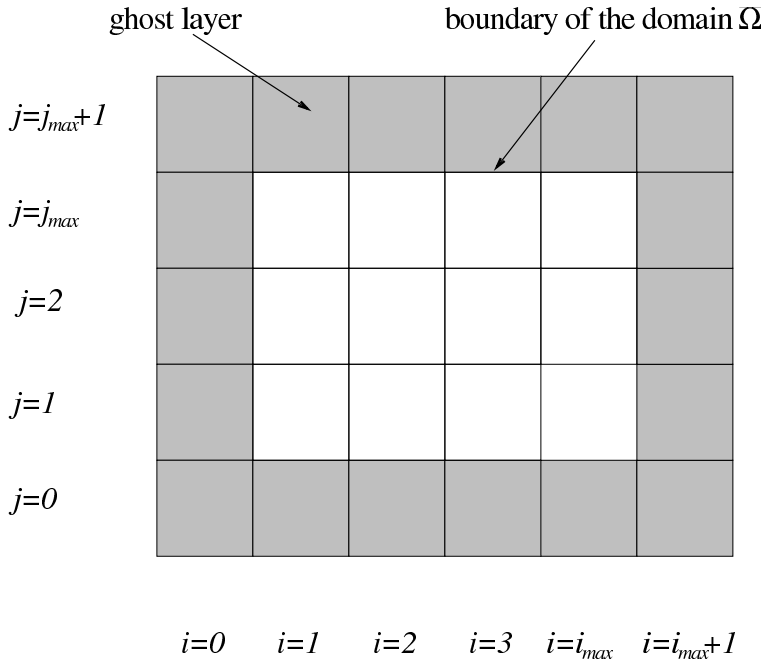

FIGURE 3.5: The computational domain including the ghost layer

$$\triangle \mathbf{u} = \nabla p \tag{3.3b}$$

3.3.1 The Discretization

As already mentioned, we want to perform all computations in a plane Cartesian co–ordinate system (x, y), so we may rewrite (3.3) in componental form,

$$\frac{\partial u}{\partial x} + \frac{\partial v}{\partial y} = 0 \tag{3.4a}$$

$$\frac{\partial^2 u}{\partial x^2} + \frac{\partial^2 u}{\partial y^2} = \frac{\partial p}{\partial x} \tag{3.4b}$$

$$\frac{\partial^2 v}{\partial x^2} + \frac{\partial^2 v}{\partial y^2} = \frac{\partial p}{\partial y} \tag{3.4c}$$

where u and v are the velocity components in x and y direction, respectively. Using the discretization formulae

$$\left[\frac{\partial u}{\partial x}\right]_{i,j} = \frac{u_{i,j} - u_{i-1,j}}{\delta x} \tag{3.5}$$

$$\left[\frac{\partial v}{\partial y}\right]_{i,j} = \frac{v_{i,j} - v_{i,j-1}}{\delta y} \tag{3.6}$$

$$\left[\frac{\partial^2 u}{\partial x^2}\right]_{i,j} = \frac{u_{i+1,j} - 2u_{i,j} + u_{i-1,j}}{(\delta x)^2} \tag{3.7}$$

$$\left[\frac{\partial^2 u}{\partial y^2}\right]_{i,j} = \frac{u_{i,j+1} - 2u_{i,j} + u_{i,j-1}}{(\delta y)^2} \tag{3.8}$$

$$\left[\frac{\partial^2 v}{\partial x^2}\right]_{i,j} = \frac{v_{i+1,j} - 2v_{i,j} + v_{i-1,j}}{(\delta x)^2} \tag{3.9}$$

$$\left[\frac{\partial^2 v}{\partial y^2}\right]_{i,j} = \frac{v_{i,j+1} - 2v_{i,j} + v_{i,j-1}}{(\delta y)^2} \tag{3.10}$$

$$\left[\frac{\partial p}{\partial x}\right]_{i,j} = \frac{p_{i+1,j} - p_{i,j}}{\delta x} \tag{3.11}$$

and

$$\left[\frac{\partial p}{\partial y}\right]_{i,j} = \frac{p_{i,j+1} - p_{i,j}}{\delta y} \tag{3.12}$$

we obtain the discrete version of (3.4),

$$\frac{u_{i,j} - u_{i-1,j}}{\delta x} + \frac{v_{i,j} - v_{i,j-1}}{\delta y} = 0 \tag{3.13a}$$

$$\frac{u_{i+1,j} - 2u_{i,j} + u_{i-1,j}}{(\delta x)^2} + \frac{u_{i,j+1} - 2u_{i,j} + u_{i,j-1}}{(\delta y)^2} = \frac{p_{i+1,j} - p_{i,j}}{\delta x} \tag{3.13b}$$

$$\frac{v_{i+1,j} - 2v_{i,j} + v_{i-1,j}}{(\delta x)^2} + \frac{v_{i,j+1} - 2v_{i,j} + v_{i,j-1}}{(\delta y)^2} = \frac{p_{i,j+1} - p_{i,j}}{\delta y} \tag{3.13c}$$

$$\text{for } i = 1 \ldots i_{max},\ j = 1 \ldots j_{max}$$

Please note that we are discretizing the continuity equation (3.4a) at the cell center using central differences with step sizes $\delta x/2$ and $\delta y/2$, while we are discretizing the momentum balance equations (3.4b) and (3.4c) at the cell edges. Therefore, we are discretizing the pressure derivatives using central differences with step sizes $\delta x/2$ and $\delta y/2$, while we are discretizing the second order derivatives of the velocity components by approximating the first order derivatives of u and v with central differences with step size $\delta x/2$ ($\delta y/2$) at $x_{1+1/2}$ and $x_{i-1/2}$ ($y_{j+1/2}$ and $y_{j-1/2}$) and afterwards using these values do approximate the second order derivatives by central differences with the same step sizes at x_i (y_j), where $x_i := i\delta x$ ($y_j := j\delta y$).

3.3.2 The Solution Scheme

To solve the system of equations (3.13), we have to apply some appropriate initial values for u, v, and p, and afterwards to perform a number of relaxation iterations for the momentum balance equations (3.13b) and (3.13c) until the system reaches its steady state. In more detail, we consider the liquid and both solids to be initially at rest, and just at the beginning of the simulation the solids start to move. Therefore, the solids force the liquid to flow (due to frictional effects). After a number of relaxation iterations, the flow system will have reached its steady state. In this connection, the role of the relaxation parameter is played by an imaginary 'time' step size. This means that we have to solve the discrete 'time'–dependent Stokes equations

$$u_{i,j}^{(n+1)} = F_{i,j}^{(n)} - \delta t \frac{p_{i+1,j}^{(n+1)} - p_{i,j}^{(n+1)}}{\delta x} \tag{3.14a}$$

$$v_{i,j}^{(n+1)} = G_{i,j}^{(n)} - \delta t \frac{p_{i,j+1}^{(n+1)} - p_{i,j}^{(n+1)}}{\delta y} \tag{3.14b}$$

for $i = 1 \ldots i_{max}, j = 1 \ldots j_{max}$, where

$$F_{i,j}^{(n)} = u_{i,j}^{(n)} + \delta t \left(\frac{u_{i+1,j}^{(n)} - 2u_{i,j}^{(n)} + u_{i-1,j}^{(n)}}{(\delta x)^2} + \frac{u_{i,j+1}^{(n)} - 2u_{i,j}^{(n)} + u_{i,j-1}^{(n)}}{(\delta y)^2} \right) \tag{3.15}$$

and

$$G_{i,j}^{(n)} = v_{i,j}^{(n)} + \delta t \left(\frac{v_{i+1,j}^{(n)} - 2v_{i,j}^{(n)} + v_{i-1,j}^{(n)}}{(\delta x)^2} + \frac{v_{i,j+1}^{(n)} - 2v_{i,j}^{(n)} + v_{i,j-1}^{(n)}}{(\delta y)^2} \right) \tag{3.16}$$

t is the 'time' variable, δt is the 'time' step, and the superscripts (n) and $(n+1)$ denote values after n and $n+1$ 'time' steps, respectively. Let us assume that the system has reached its steady state if the discrete $\mathcal{L}^2$–norms of $(u^{(n+1)} - u^{(n)})$, $(v^{(n+1)} - v^{(n)})$, and $(p^{(n+1)} - p^{(n)})$ are smaller than a given value ϵ_1,

$$\left\| \left(u^{(n+1)} - u^{(n)} \right) \right\|_2 = \sqrt{\frac{1}{i_{max} j_{max}} \sum_{i=1}^{i_{max}} \sum_{j=1}^{j_{max}} \left(u_{i,j}^{(n+1)} - u_{i,j}^{(n)} \right)^2} < \epsilon_1 \tag{3.17}$$

$$\left\| \left(v^{(n+1)} - v^{(n)} \right) \right\|_2 = \sqrt{\frac{1}{i_{max} j_{max}} \sum_{i=1}^{i_{max}} \sum_{j=1}^{j_{max}} \left(v_{i,j}^{(n+1)} - v_{i,j}^{(n)} \right)^2} < \epsilon_1 \tag{3.18}$$

and

$$\left\| \left(p^{(n+1)} - p^{(n)} \right) \right\|_2 = \sqrt{\frac{1}{i_{max} j_{max}} \sum_{i=1}^{i_{max}} \sum_{j=1}^{j_{max}} \left(p_{i,j}^{(n+1)} - p_{i,j}^{(n)} \right)^2} < \epsilon_1 \tag{3.19}$$

It is very convenient to assume that the liquid is in equilibrium before the solids start to move, and therefore the natural choice of initial conditions for the above numerical method is

$$u_{i,j} = v_{i,j} = p_{i,j} = 0 \tag{3.20}$$

at $t = 0$ for $i = 0 \ldots i_{max} + 1, j = 0 \ldots j_{max} + 1$

Sometimes, numerical calculations compute solutions strongly oscillating in space, time, or both of them, even though the physical problem being studied

is known to have no unstable solutions. This phenomenon is called numerical instability. To guarantee that a numerical method is always stable, one must pose some conditions for δx, δy, and δt. In case of the 'time'–dependent incompressible Navier–Stokes equations, the mostly used stability criteria are [7]

$$\|u\|_{max}\,\delta t < \delta x \tag{3.21}$$

$$\|v\|_{max}\,\delta t < \delta y \tag{3.22}$$

and

$$\frac{2\delta t}{Re} < \left(\frac{1}{(\delta x)^2} + \frac{1}{(\delta y)^2}\right)^{-1} \tag{3.23}$$

where $\|u\|_{max}$ and $\|v\|_{max}$ are the maximum norms of the velocity components,

$$\|u\|_{max} = \max_{\substack{i=0\ldots i_{max}+1\\ j=0\ldots j_{max}+1}} |u_{i,j}| \tag{3.24}$$

and

$$\|v\|_{max} = \max_{\substack{i=0\ldots i_{max}+1\\ j=0\ldots j_{max}+1}} |v_{i,j}| \tag{3.25}$$

Conditions (3.21) and (3.22) are to make sure that no material point moves through more than one grid cell in one 'time' step, and condition (3.23) is to keep momentum from diffusing more than approximately one cell in one 'time' step. Since the Stokes equations are independent of the Reynolds number Re, it is convenient to replace (3.23) with some criterion independent of Re. To find such a criterion, several numerical experiments were performed, and those experiments clearly proposed that

$$2\delta t < \left(\frac{1}{(\delta x)^2} + \frac{1}{(\delta y)^2}\right)^{-1} \tag{3.26}$$

is a very good choice. To make sure that the stability criteria (3.21), (3.22), and (3.26) are fulfilled, we will compute the 'time' step size adaptively at each 'time' step, i.e. we will calculate δt from the formula

$$\delta t := \nu \min\left\{\frac{1}{2}\left(\frac{1}{(\delta x)^2} + \frac{1}{(\delta y)^2}\right)^{-1}, \frac{\delta x}{\|u\|_{max}}, \frac{\delta y}{\|v\|_{max}}\right\} \tag{3.27}$$

where $\nu \in\,]0, 1]$ is a security factor applied to make sure that the right hand sides of all three stability criteria (3.21), (3.22), and (3.26) are greater than (and not equal to) the left hand sides.

3.3.3 The Poisson Equation for p

Due to the solution strategy described in subsection 3.3.2, we have to compute the pressure at the new 'time' level before we can calculate the new velocity components, and we will do so by exploiting the continuity equation (3.13a) after $n+1$ 'time' steps. Proceeding like this, we make sure that (3.13a) is always fulfilled at a given time step. Let us therefore put (3.14a) and (3.14b) into (3.13a) at the $(n+1)^{\text{st}}$ time step. This results in

$$\frac{F_{i,j}^{(n)} - F_{i-1,j}^{(n)}}{\delta x} - \delta t \frac{p_{i+1,j}^{(n+1)} - 2p_{i,j}^{(n+1)} + p_{i-1,j}^{(n+1)}}{(\delta x)^2}$$

$$+ \frac{G_{i,j}^{(n)} - G_{i,j-1}^{(n)}}{\delta y} - \delta t \frac{p_{i,j+1}^{(n+1)} - 2p_{i,j}^{(n+1)} + p_{i,j-1}^{(n+1)}}{(\delta y)^2} = 0$$

$$\text{for } i = 1 \ldots i_{max}, j = 1 \ldots j_{max} \quad (3.28)$$

which we can rewrite as

$$\frac{p_{i+1,j}^{(n+1)} - 2p_{i,j}^{(n+1)} + p_{i-1,j}^{(n+1)}}{(\delta x)^2} + \frac{p_{i,j+1}^{(n+1)} - 2p_{i,j}^{(n+1)} + p_{i,j-1}^{(n+1)}}{(\delta y)^2}$$

$$= \frac{1}{\delta t} \left(\frac{F_{i,j}^{(n)} - F_{i-1,j}^{(n)}}{\delta x} + \frac{G_{i,j}^{(n)} - G_{i,j-1}^{(n)}}{\delta y} \right)$$

$$\text{for } i = 1 \ldots i_{max}, j = 1 \ldots j_{max} \quad (3.29)$$

(3.29) defines a discrete Poisson equation for the pressure because

$$[\triangle p]_{i,j} = \frac{p_{i+1,j} - 2p_{i,j} + p_{i-1,j}}{(\delta x)^2} + \frac{p_{i,j+1} - 2p_{i,j} + p_{i,j-1}}{(\delta y)^2} \quad (3.30)$$

is a valid discretization formula for $\triangle p$, obtained in the same way as the discretization formulae for the second order derivatives of the velocity components in subsection 3.3.1. After applying some appropriate boundary conditions, we may now solve equation (3.29) numerically.

Formally, we must impose some boundary conditions to solve equation (3.29). In particular, we have to prescribe

$$p_{0,j}^{(n+1)}, p_{i_{max}+1,j}^{(n+1)}, F_{0,j}^{(n)}, \text{ and } F_{i_{max},j}^{(n)} \qquad \text{for } j = 1, \ldots, j_{max}$$

and

$$p_{i,0}^{(n+1)}, p_{i,j_{max}+1}^{(n+1)}, G_{i,0}^{(n)}, \text{ and } G_{i,j_{max}}^{(n)} \qquad \text{for } i = 1, \ldots, i_{max}$$

To get appropriate values for these boundary conditions, we may now rewrite the discrete 'time'–dependent Stokes equations (3.14) in vector form and then form the scalar product of both sides of the resulting vector equation at the boundary Γ with the inner normal vector $\mathbf{n} = (n_x, n_y)^T$ to Γ, so we get

$$\left(\begin{array}{c} \frac{p_{i+1,j}^{(n+1)} - p_{i,j}^{(n+1)}}{\delta x} \\ \frac{p_{i,j+1}^{(n+1)} - p_{i,j}^{(n+1)}}{\delta y} \end{array} \right) \Bigg|_{\Gamma} \cdot \mathbf{n} = \left(\begin{array}{c} F_{i,j}^{(n)} - u_{i,j}^{(n+1)} \\ G_{i,j}^{(n)} - v_{i,j}^{(n+1)} \end{array} \right) \Bigg|_{\Gamma} \cdot \mathbf{n} \tag{3.31}$$

and returning to componental notation we obtain from (3.31)

$$\begin{aligned} &\frac{p_{i+1,j}^{(n+1)} - p_{i,j}^{(n+1)}}{\delta x} \Bigg|_{\Gamma} n_x + \frac{p_{i,j+1}^{(n+1)} - p_{i,j}^{(n+1)}}{\delta y} \Bigg|_{\Gamma} n_y \\ &\qquad = -\frac{1}{\delta t} \left(\left[u_{i,j}^{(n+1)} - F_{i,j}^{(n)} \right]_{\Gamma} n_x + \left[v_{i,j}^{(n+1)} - G_{i,j}^{(n)} \right]_{\Gamma} n_y \right) \end{aligned} \tag{3.32}$$

Performing this calculation for all boundaries of the computational domain, i.e. $\mathbf{n} = (1,0)^T, (-1,0)^T, (0,1)^T, (0,-1)^T$ for the left ($i = 0$), right ($i = i_{max}$), lower ($j = 0$), and upper ($j = j_{max}$) boundary, respectively, yields

$$\frac{p_{0,j}^{(n+1)} - p_{1,j}^{(n+1)}}{\delta x} = \frac{1}{\delta t} \left(u_{0,j}^{(n+1)} - F_{0,j}^{(n)} \right) \qquad \text{for } j = 1, \ldots, j_{max} \tag{3.33}$$

$$\frac{p_{i_{max},j}^{(n+1)} - p_{i_{max}+1,j}^{(n+1)}}{\delta x} = \frac{1}{\delta t} \left(u_{i_{max},j}^{(n+1)} - F_{i_{max},j}^{(n)} \right) \qquad \text{for } j = 1, \ldots, j_{max} \tag{3.34}$$

$$\frac{p_{i,0}^{(n+1)} - p_{i,1}^{(n+1)}}{\delta y} = \frac{1}{\delta t} \left(v_{i,0}^{(n+1)} - G_{i,0}^{(n)} \right) \qquad \text{for } i = 1, \ldots, i_{max} \tag{3.35}$$

and

$$\frac{p_{i,j_{max}}^{(n+1)} - p_{i,j_{max}+1}^{(n+1)}}{\delta y} = \frac{1}{\delta t} \left(v_{i,j_{max}}^{(n+1)} - G_{i,j_{max}}^{(n)} \right) \qquad \text{for } i = 1, \ldots, i_{max} \tag{3.36}$$

Solving (3.33) for $F_{0,j}^{(n)}$, (3.34) for $F_{i_{max},j}^{(n)}$, (3.35) for $G_{i,0}^{(n)}$, and (3.36) for $G_{i,j_{max}}^{(n)}$ and then putting the results into (3.29) for $i = 1$, $i = i_{max}$, $j = 1$, and $j = j_{max}$, respectively, we obtain

$$\frac{p_{2,j}^{(n+1)} - p_{1,j}^{(n+1)}}{(\delta x)^2} + \frac{p_{1,j+1}^{(n+1)} - 2p_{1,j}^{(n+1)} + p_{1,j-1}^{(n+1)}}{(\delta y)^2}$$

$$= \frac{1}{\delta t}\left(\frac{F_{1,j}^{(n)} - u_{0,j}^{(n+1)}}{\delta x} + \frac{G_{1,j}^{(n)} - G_{1,j-1}^{(n)}}{\delta y}\right) \quad (3.37)$$

$$\frac{p_{imax-1,j}^{(n+1)} - p_{imax,j}^{(n+1)}}{(\delta x)^2} + \frac{p_{imax,j+1}^{(n+1)} - 2p_{imax,j}^{(n+1)} + p_{imax,j-1}^{(n+1)}}{(\delta y)^2}$$

$$= \frac{1}{\delta t}\left(\frac{u_{imax,j}^{(n+1)} - F_{imax-1,j}^{(n)}}{\delta x} + \frac{G_{imax,j}^{(n)} - G_{imax,j-1}^{(n)}}{\delta y}\right) \quad (3.38)$$

$$\frac{p_{i+1,1}^{(n+1)} - 2p_{i,1}^{(n+1)} + p_{i-1,1}^{(n+1)}}{(\delta x)^2} + \frac{p_{i,2}^{(n+1)} - p_{i,1}^{(n+1)}}{(\delta y)^2}$$

$$= \frac{1}{\delta t}\left(\frac{F_{i,1}^{(n)} - F_{i-1,1}^{(n)}}{\delta x} + \frac{G_{i,1}^{(n)} - v_{i,0}^{(n+1)}}{\delta y}\right) \quad (3.39)$$

and

$$\frac{p_{i+1,jmax}^{(n+1)} - 2p_{i,jmax}^{(n+1)} + p_{i-1,jmax}^{(n+1)}}{(\delta x)^2} + \frac{p_{i,jmax-1}^{(n+1)} - p_{i,jmax}^{(n+1)}}{(\delta y)^2}$$

$$= \frac{1}{\delta t}\left(\frac{F_{i,jmax}^{(n)} - F_{i-1,jmax}^{(n)}}{\delta x} + \frac{v_{i,jmax}^{(n+1)} - G_{i,jmax-1}^{(n)}}{\delta y}\right) \quad (3.40)$$

Looking at (3.37) – (3.40), we find that (3.29) is independent of the values of F and G at the boundaries. Therefore, we may choose some arbitrary boundary values for F and G, and we take

$$F_{0,j}^{(n)} = u_{0,j}^{(n+1)} \qquad \text{for } j = 1, \ldots, j_{max} \quad (3.41)$$

$$F_{imax,j}^{(n)} = u_{imax,j}^{(n+1)} \qquad \text{for } j = 1, \ldots, j_{max} \quad (3.42)$$

$$G_{i,0}^{(n)} = v_{i,0}^{(n+1)} \qquad \text{for } i = 1, \ldots, i_{max} \quad (3.43)$$

and

$$G^{(n)}_{i,j_{max}} = v^{(n+1)}_{i,j_{max}} \qquad \text{for } i = 1, \ldots, i_{max} \tag{3.44}$$

and sustitute the values (3.41) – (3.44) into (3.33) – (3.36), respectively. This yields the boundary conditions for the pressure,

$$p^{(n+1)}_{0,j} = p^{(n+1)}_{1,j} \qquad \text{for } j = 1, \ldots, j_{max} \tag{3.45}$$

$$p^{(n+1)}_{i_{max}+1,j} = p^{(n+1)}_{i_{max},j} \qquad \text{for } j = 1, \ldots, j_{max} \tag{3.46}$$

$$p^{(n+1)}_{i,0} = p^{(n+1)}_{i,1} \qquad \text{for } i = 1, \ldots, i_{max} \tag{3.47}$$

and

$$p^{(n+1)}_{i,j_{max}+1} = p^{(n+1)}_{i,j_{max}} \qquad \text{for } i = 1, \ldots, i_{max} \tag{3.48}$$

Now we may solve equation (3.29) using the SOR–method [7]

for $i = 1 \ldots i_{max}$ do

for $j = 1 \ldots j_{max}$ do

$$p^{k+1}_{i,j} := (1-\omega) + \frac{\omega}{\left(\frac{2}{(\delta x)^2} + \frac{2}{(\delta y)^2}\right)} \cdot \left(\frac{p^{k}_{i+1,j} + p^{k+1}_{i-1,j}}{(\delta x)^2} + \frac{p^{k}_{i,j+1} + p^{k+1}_{i,j-1}}{(\delta y)^2} - rhs_{i,j} \right) \tag{3.49}$$

where $rhs_{i,j}$ stands for the right hand side of the pressure equation (3.29) in cell (i,j), and $\omega \in [0,2]$ is a relaxation parameter frequently chosen to be $\omega = 1.7$. Please note that we have to set the boundary conditions for the pressure before each iteration of the SOR method (3.49), i.e.

$$p^{k+1}_{0,j} = p^{k}_{1,j} \qquad \text{for } j = 1, \ldots, j_{max} \tag{3.50}$$

$$p^{k+1}_{i_{max}+1,j} = p^{k}_{i_{max},j} \qquad \text{for } j = 1, \ldots, j_{max} \tag{3.51}$$

$$p^{k+1}_{i,0} = p^{k}_{i,1} \qquad \text{for } i = 1, \ldots, i_{max} \tag{3.52}$$

and

$$p^{k+1}_{i,j_{max}+1} = p^k_{i,j_{max}} \qquad \text{for } i = 1, \ldots, i_{max} \tag{3.53}$$

This procedure of setting the pressure boundary conditions leads to a stable numerical method, and we do not expect any difficulties as they may appear with other choices of the pressure boundary conditions [7]. Let us finally define the residual $r^k_{i,j}$ of the SOR method (3.49) as

$$r^k_{i,j} := \frac{p^k_{i+1,j} - 2p^k_{i,j} + p^k_{i-1,j}}{(\delta x)^2} + \frac{p^k_{i,j+1} - 2p^k_{i,j} + p^k_{i,j-1}}{(\delta y)^2} - rhs_{i,j}$$

$$\text{for } i = 1 \ldots i_{max}, j = 1 \ldots j_{max} \tag{3.54}$$

and stop the iterations of the SOR method (3.49) either after a given number of iterations k_{max} or if the discrete $\mathcal{L}^2$–norm of the residual is smaller than a given value ϵ_2,

$$\left\| r^k \right\|_2 = \sqrt{\frac{1}{i_{max} j_{max}} \sum_{i=1}^{i_{max}} \sum_{j=1}^{j_{max}} \left(r^k_{i,j} \right)^2} < \epsilon_2 \tag{3.55}$$

3.4 The Treatment of the Free Liquid Surface

We want to use a level set method [12, 16] to mark the position and the shape of the free liquid surface. Let us therefore define the values of the level set function $\Phi(x, y)$ to be the distance of the point $(x, y)^T \in \mathbb{R}^2$ from the free liquid surface. Thus, the zero level set of Φ, i.e. the set of points $(\tilde{x}, \tilde{y}) \in \mathbb{R}^2$ where $\Phi(\tilde{x}, \tilde{y}) = 0$, is exactly the free surface of the liquid. We will consider Φ at the cell centers, i.e. $\Phi_{i,j}$ will denote the value of Φ at the center of cell (i, j). In other words, the level set function is considered at the same points as the pressure field (see again Figure 3.4). Please remember that we are working in a co–ordinate frame fixed with respect to the moving contact line, and therefore the liquid front does not change its position with respect to the computational grid. Thus, we are free to choose the position of the moving contact lines with respect to the grid, and we decide to locate them at

$$x_{mcl} := \frac{i_{max} + 1}{2} \delta x \tag{3.56}$$

Defining the shape of the free liquid surface, we have to take care about the dynamic contact angle θ_d which we have to calculate from (2.226). To construct a

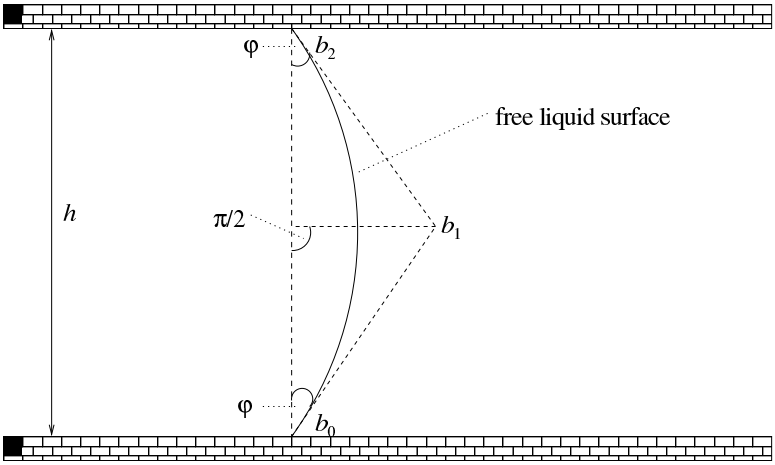

FIGURE 3.6: The quantities needed for the Bézier method

liquid front with dynamic contact angle θ_d at both solid boundaries, let us define the free liquid surface as a Bézier spline [5, 11] with Bézier points

$$b_0 = 0 \tag{3.57}$$

$$b_1 = \frac{h}{2} \tan \varphi \tag{3.58}$$

and

$$b_2 = 0 \tag{3.59}$$

See Figure 3.6 for the definitions of h and φ, and please note that $\varphi = \theta_d - \pi/2$. From $b_0 = b_2 = 0$ follows that

$$P(\eta) := b_1 B_1^2(\eta) \tag{3.60}$$

is the difference of the x values of the liquid front and the moving contact line(s), where

$$B_1^2(\eta) := 2\eta(1-\eta) \tag{3.61}$$

denotes the first Bernstein polynomial of degree two, and

$$\eta = \frac{y}{h} \tag{3.62}$$

Thus, we may compute the x value of the free liquid front at a given y by adding $P(\eta)$ to x_{mcl}. Summarizing these results, we end up with the following formula for the computation of the x co–ordinate of the free liquid surface at a given y:

$$x_{front} := x_{mcl} + h\eta \tan\varphi\,(1-\eta) \tag{3.63}$$

where x_{front} denotes the x value of the liquid front at a given y.

Let us now introduce a flag field to mark each cell inside the computational domain Ω. The flag field can take the following values to describe the character of a given cell:

C_B	boundary cell
C_E	empty cell
C_F	liquid ('fluid') cell
C_N	liquid cell whose upper ('northern') neighbouring cell is empty
C_S	liquid cell whose lower ('southern') neighbouring cell is empty
C_O	liquid cell whose right ('eastern') neighbouring cell is empty
C_W	liquid cell whose left ('western') neighbouring cell is empty
C_{NS}	liquid cell whose upper and lower neighbouring cells are empty
C_{NO}	liquid cell whose upper and right neighbouring cells are empty
C_{NW}	liquid cell whose upper and left neighbouring cells are empty
C_{WO}	liquid cell whose left and right neighbouring cells are empty
C_{SO}	liquid cell whose lower and right neighbouring cells are empty
C_{SW}	liquid cell whose lower and left neighbouring cells are empty
C_{NWO}	liquid cell whose upper, left, and right neighbouring cells are empty
C_{NSW}	liquid cell whose upper, left, and lower neighbouring cells are empty
C_{SWO}	liquid cell whose lower, left, and right neighbouring cells

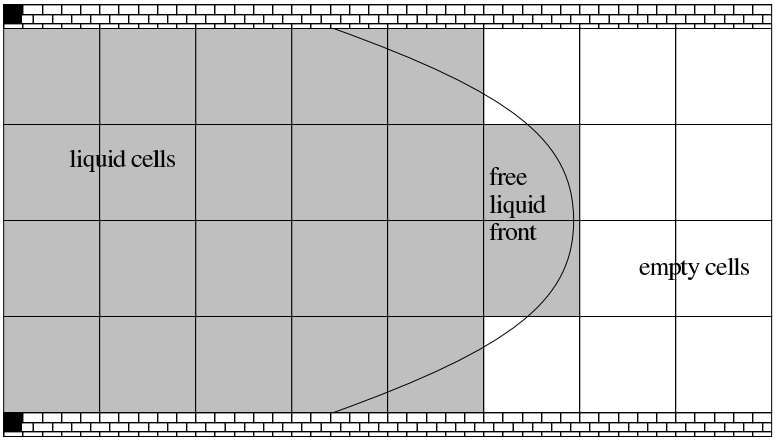

FIGURE 3.7: The exact shape of the free liquid surface and its approximation by cell edges

are empty

C_{NSWO} liquid cell with four empty neighbouring cells

(Some cell types, e.g. C_{NSWO}, do not appear in a channel inflow simulation, but we want to keep them as theoretically possible values of the flag field in order to keep the method open for future generalization.) We choose to treat each non–boundary cell with $\Phi_{i,j} < (1/2) \cdot \delta x$ or $\Phi_{i,j} < (1/2) \cdot \delta y$ as a liquid cell and all the other non–boundary cells as empty cells. Using this technique, we are approximating the shape of the free liquid front by a combination of cell fronts. Figure 3.7 gives an illustration of the approximated shape of the free liquid surface.

The last thing to be done in this section is the proper establishment of the slip regions around the moving contact. Please remember that we want to have fairly small slip regions because we want the liquid front in each slip region to be free from the influence of the solid on the opposite side of the liquid domain. Let us therefore define each slip region to be the one grid cell inside the liquid domain which contains the moving contact line at the corresponding solid (see Figure 3.8).

3.5 The Boundary Conditions for the Flow Field

This section deals with the boundary conditions for the numerical scheme (3.14) for the computation of the velocity field. Please remember that we want to treat a flow system where the liquid is initially at rest and the flow is caused by the solids moving along the liquid boundaries. Furthermore, we should keep in mind that the speed of the solid(s) is the characteristic speed of the flow system. According to the mathematical model described in Chapter 2, we have to consider

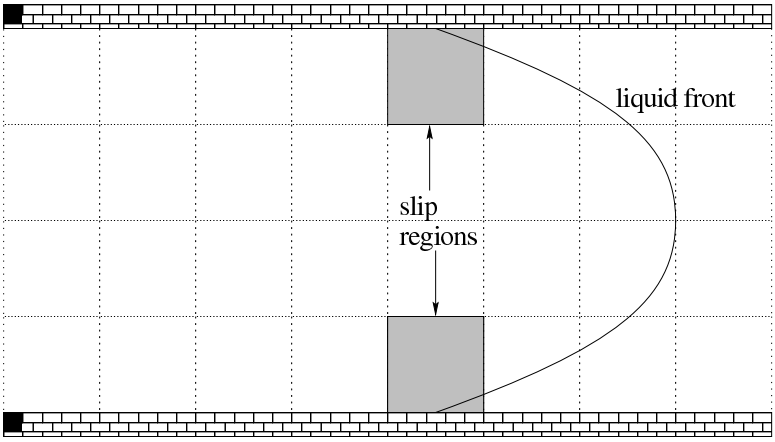

FIGURE 3.8: The numerical slip regions inside the channel

the following boundary types:

- the 'inflow' boundary
- the solid boundaries of the 'outer' asymptotic region.
- the free boundary of the 'outer' asymptotic region.
- the solid boundaries of the 'intermediate' asymptotic region.
- the free boundary of the 'intermediate' asymptotic region.
- the 'outflow' boundary

3.5.1 The 'Inflow' Boundary

Far from the free liquid surface, we want the flow field to be identical to the flow field of a fully developed flow in a channel completely filled with liquid, and thus to be constant with respect to x. Using the fact that the x direction is the normal direction to the inflow boundary (the boundary marked as Γ_{in} in Figure 1.1), we force the normal derivative of u and v to be zero at the 'inflow' boundary. This yields

$$u_{0,j} = u_{1,j} \tag{3.64}$$

$$v_{0,j} = v_{1,j} \tag{3.65}$$

3.5.2 Solid Boundaries of the Bulk

At this stage, everything goes straightforward: We imply the usual no–slip boundary condition (2.109), i.e. $u = -1$ and $v = 0$, at the solid walls. The solid walls are horizontal boundaries, and thus we do not have any grid points for the values of u along them (see Figure 3.4). Let us therefore use the technique of linear extrapolation to set the boundary conditions for u along the solid walls [7]. Therefore, the conditions for the solid boundaries of the liquid bulk are

$$u_{i,0} = -2 - u_{i,1} \tag{3.66}$$

$$v_{i,0} = 0 \tag{3.67}$$

and

$$u_{i,j_{max}+1} = -2 - u_{i,j_{max}} \tag{3.68}$$

$$v_{i,jmax} = 0 \tag{3.69}$$

3.5.3 The Slip Region

In the slip region, we have to apply (2.218) and (2.219) at the solid surface, as well as (2.220) and (2.221) along the liquid front. Please note that we have two moving contact lines, one at each solid wall, and at both those moving contact lines the liquid particles at the free surface must flow towards the contact line, not away from it. This behaviour must be considered during the transformation of (2.220) to the Cartesian co–ordinate frame used here.

We want each slip region to consist of exactly one grid cell, so we have to apply the conditions mentioned above exactly to those two grid cells which contain the moving contact lines. Therefore, we must set the Cartesian velocity components u and v in the relevant grid cells in such a way that (2.218) – (2.221) are fulfilled. This yields

$$u_{\tilde{i},1} = -2u_{r(0)}(\theta_d)\cos\theta_d - u_{\tilde{i}-1,1} \tag{3.70}$$

$$u_{\tilde{i},0} = -2u_{r(0)} - u_{\tilde{i},1} \tag{3.71}$$

$$v_{\tilde{i},1} = 2u_{r(0)}(\theta_d)\sin\theta_d - v_{\tilde{i},0} \tag{3.72}$$

and

$$u_{\tilde{i},j_{max}} = -2u_{r(0)}(\theta_d)\cos\theta_d - u_{\tilde{i}-1,j_{max}} \tag{3.73}$$

$$u_{\tilde{i},j_{max}+1} = -2u_{r(0)} - u_{\tilde{i},j_{max}} \tag{3.74}$$

$$v_{\tilde{i},j_{max}-1} = 2u_{r(0)}(\theta_d)\sin\theta_d - v_{\tilde{i},j_{max}} \tag{3.75}$$

where $(\tilde{i}, 1)$ and $(\tilde{i}, j_{max})$ denote the grid cells representing the slip regions around the lower and upper contact line, respectively, and r is the radial co–ordinate of the grid point(s) where we want to force u to fulfill the conditions at the solid boundaries in the co–ordinate frame used in chapter 2. Thus, r is nothing but the distance between this grid point and the moving contact line. Please note that $u_{\tilde{i},1}$ and $u_{\tilde{i},j_{max}}$ must be set before $u_{\tilde{i},0}$ and $u_{\tilde{i},j_{max}+1}$, respectively, because otherwise the values of the latter two will not be correct. The boundary conditions (3.70) – (3.75) are the core of the numerical method presented in this chapter because they are the main difference between this method and the classical numerical treatment of a channel flow.

3.5.4 The Free Surface of the Bulk and the 'Outflow' Boundary

The influence of the free surface in the vicinity of the moving contact line combined with the influence of the solid boundaries will force the correct flow field at the free surface of the liquid bulk, so we do not prescribe any conditions for the velocity field here.

Due to the choice of a coordinate system fixed with respect to the moving contact line, no liquid will ever reach the outflow boundary of the computational domain (the boundary marked as Γ_{out} in figure 1.1). Therefore, we do not need to take care for any boundary conditions for the velocity field along the outflow.

3.6 The Basic Features of the Problem Solver

3.6.1 The Problem Parameters

To implement the model properly, we need to deal with the following problem parameters:

- the domain length a in x direction,
- the domain length b in y direction,
- the number of grid cells i_{max} in x direction,
- the number of grid cells j_{max} in y direction,
- the stopping parameter ϵ_1 for the 'time' iterations of the Stokes equations,

- the step size δx in x direction,
- the step size δy in y direction,
- the security factor ν for the calculation of the time step,
- the maximum number of iterations k_{max} for the pressure correction,
- the stopping parameter ϵ_2 for the pressure correction,
- the relaxation parameter ω for the SOR method,
- the static contact angle θ_s,
- the dynamic contact angle θ_d,
- the system constants A, B, q, and V,
- the equilibrium density ρ_f^s of the free liquid surface, and
- the equilibrium density ρ_s^s of the solid surfaces of the liquid domain.

We can reduce the number of parameters by applying the following knowledge: We know that $A = 1/12$ for channel flows [13], and we have the formulae (3.2) to compute δx and δy, equations (2.224) and (2.225) to get q and B, respectively, equations (2.227) and (2.228) to express λ and ρ_s^s, respectively, and finally, in order to compute θ_d we can use equation (2.212) to define the function

$$f(\theta_d) := \cos\theta_s - \cos\theta_d - \lambda\left(\rho_s^s + \rho_f^s u_{r(0)}(\theta_d)\right)\left(\frac{q}{4V^2} + 1\right)^{-1} \tag{3.76}$$

and afterwards solve the equation

$$f(\theta_d) = 0 \tag{3.77}$$

numerically by applying Newton's algorithm [5, 11] (often referred to as the Newton–Raphson algorithm), i.e. by applying the iteration formula

$$\theta_d^{(m+1)} = \theta_d^{(m)} - \frac{f\left(\theta_d^{(m)}\right)}{f'\left(\theta_d^{(m)}\right)} \tag{3.78}$$

where m is the iteration counter and $f' = \partial f/\partial\theta_d$. A suitable initial value is $\theta_d = \theta_s$. It is convenient to stop iterating (3.78) if the absolute value of the difference between $\theta_d^{(m+1)}$ and $\theta_d^{(m)}$ is smaller than a prescribed value ϵ_3,

$$\left|\theta_d^{(m+1)} - \theta_d^{(m)}\right| < \epsilon_3 \tag{3.79}$$

The Newton algorithm surely diverges if

$$\left|\frac{f(\theta_d^{(m+1)})}{f'(\theta_d^{(m)})}\right| > \frac{1}{2}\left|\frac{f(\theta_d^{(m)})}{f'(\theta_d^{(m)})}\right| \tag{3.80}$$

Including this divergence check into the numerical method and introducing the shortcuts

$$\Delta\theta_d^{(m)} := -\frac{f\left(\theta_d^{(m)}\right)}{f'\left(\theta_d^{(m)}\right)} \tag{3.81}$$

and

$$\bar{\Delta}\theta_d^{(m+1)} := -\frac{f\left(\theta_d^{(m+1)}\right)}{f'\left(\theta_d^{(m)}\right)} \tag{3.82}$$

we gain the following algorithm for the computation of θ_d:

1. let $m := 0$, $\theta_d^{(0)} := \theta_s$, $\Delta\theta_d^{(0)} := 100$, and $f'\left(\theta_d^{(0)}\right) := 1$
2. **begin of the iteration loop**
   (a) compute $f\left(\theta_d^{(m+1)}\right)$
   (b) **if** $\left|\bar{\Delta}\theta_d^{(m+1)}\right| > \left|\Delta\theta_d^{(m)}\right|$
   stop the program: divergence of the Newton algorithm
   else go on with 2c
   (c) compute $f'\left(\theta_d^{(m+1)}\right)$
   (d) let $\theta_d^{(m+1)} = \theta_d^{(m)} + \Delta\theta_d^{(m)}$
   (e) **if** $\left|\theta_d^{(m+1)} - \theta_d^{(m)}\right| < \epsilon 3$ go on with 3,
   else increase m by one and return to 2a
3. return $\theta_d^{(m+1)}$

Therefore, the parameters we have to declare are

$$a, b, i_{max}, j_{max}, \epsilon_1, \delta t, \nu, k_{max}, \epsilon_2, \omega, \theta_s, V, \rho_f^s, p_S^s, \text{ and } \epsilon_3$$

where we need p_S^s for computing ρ_s^s from (2.228) and ϵ_3 for (3.79). It is very convenient to read the all the parameters listed above from an input file. Additionally, we have

$$A = \frac{1}{12} \tag{3.83}$$

for channel flows, and applying our knowledge so far we can compute

$$\delta x, \delta y, \lambda, \rho_s^s, q, B, \text{ and } \theta_d$$

3.6.2 A Sketch of the Complete Algorithm

Summarizing the results of this chapter, we can establish the following numerical algorithm for Stokes flow into an empty channel:

1. read the input file, compute the remaining parameters
2. define the x coordinate of the moving contact line(s), compute the shape of the free surface, initialize the level set function and the flag field
3. set all the boundary conditions for the velocity field
4. **begin of the 'time' loop**
   (a) compute the 'time' step size
   (b) compute $F^{(n)}$ according to (3.15) and $G^{(n)}$ according to (3.16)
   (c) compute $p^{(n+1)}$ according to (3.49)
   (d) compute $u^{(n+1)}$ and $v^{(n+1)}$ according to (3.14)
   (e) re–set all the boundary conditions for the velocity field
   (f) **if** $\left\|\left(u^{(n+1)} - u^{(n)}\right)\right\|_2 < \epsilon_1$, $\left\|\left(v^{(n+1)} - v^{(n)}\right)\right\|_2 < \epsilon_1$, and $\left\|\left(p^{(n+1)} - p^{(n)}\right)\right\|_2 < \epsilon_1$ go on with 5,
   else return to 4a
5. write $u^{(n)}$, $v^{(n)}$ and $p^{(n)}$ into the appropriate output files

Chapter 4

Some Numerical Results

In this chapter, we will have a look at some results obtained with the numerical method described in Chapter 3. The source code was implemented by the author in ANSI C on a Hewlett Packard 9000 series 700 workstation running HP–UX. the GNU C Compiler gcc V2.7 was used for compilation and the commercial software package Matlab® version 5.1.0.421 by the MathWorks inc. was used to produce the plots.

For all the simulations considered here, the computational domain consists of a channel fragment with dimensionless length $a = 4.0$ and dimensionless width $b = 1.0$ (because the channel width was chosen to be the characteristic length of the flow system). Furthermore, all results presented in this chapter were computed for

$$\epsilon_1 = 0.001,$$

$$\nu = 0.9,$$

$$k_{max} = 300,$$

$$\epsilon_2 = 0.001,$$

$$\omega = 1.7,$$

$$\theta_s = 90^{\circ},$$

$$V = 0.1,$$

$$\rho_f^s = 0.99,$$

$$p_S^s = 0,$$

$$A = 1/12, \text{ and}$$

$$\epsilon_3 = 0.001,$$

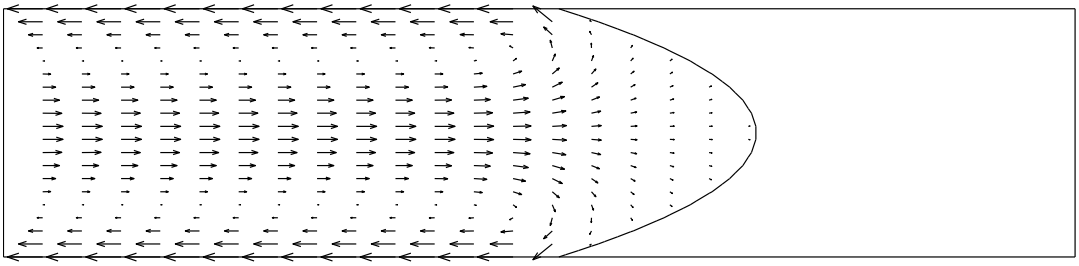

FIGURE 4.1: The velocity field computed on an 80×20 grid

and therefore

$$\rho_s^s = 1.0,$$

$$q \approx 0.1908,$$

$$B \approx -0.9592, \text{ and}$$

$$\theta_d \approx 162.5^{\circ}.$$

The computation of θ_d took four iterations. Please note that throughout this chapter, the 'time' step size δt will always be given in dimensionless form. The influence of θ_s, V, ρ_f^s, and p_S^s is discussed in [13]

We will first have a look at some results obtained on a rather coarse and a fairly fine computational grid (Sections 4.1 and 4.2, respectively), and then we will discuss some observations made during the performance of the numerical experiments (Section 4.3).

4.1 On an 80×20 Grid

Figures 4.1 – 4.4 show the velocity field, its components u and v, and the pressure distribution, respectively, inside the channel fragment Ω, as computed on an 80×20 grid. The whole simulation took 134 'time' iterations of the discrete 'time'–dependent Stokes equations (3.14), and the 'time' step computed with (3.27) proved to be constant, namely $\delta t = 5.6 \cdot 10^{-4}$.

In Figure 4.2, we can see two small areas close to the moving contact lines where the velocity outside the liquid domain in non–zero. This happens due to the numerical approximation of the liquid front as a combination of cell fronts (see Section 3.4), i.e. the code treats this area as part of the liquid domain even though it is physically outside of it. Furthermore, it is clearly visible from the plots that at a fairly short distance from the liquid front we already have a parabolic velocity field constant with respect to x and with no flow in y direction, and a pressure

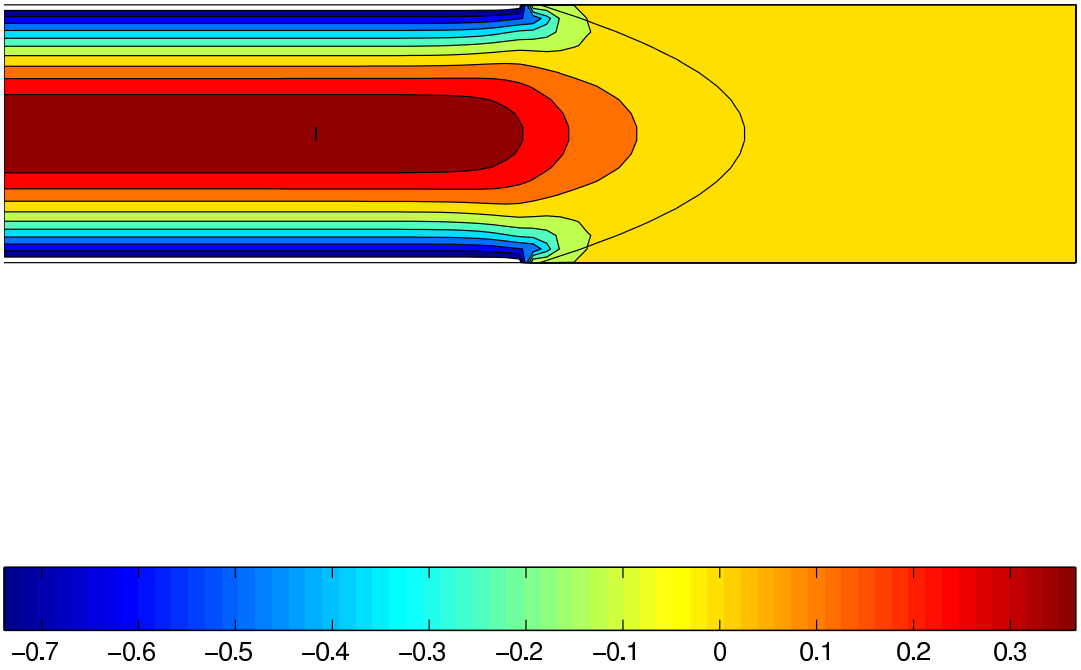

FIGURE 4.2: u computed on an 80×20 grid

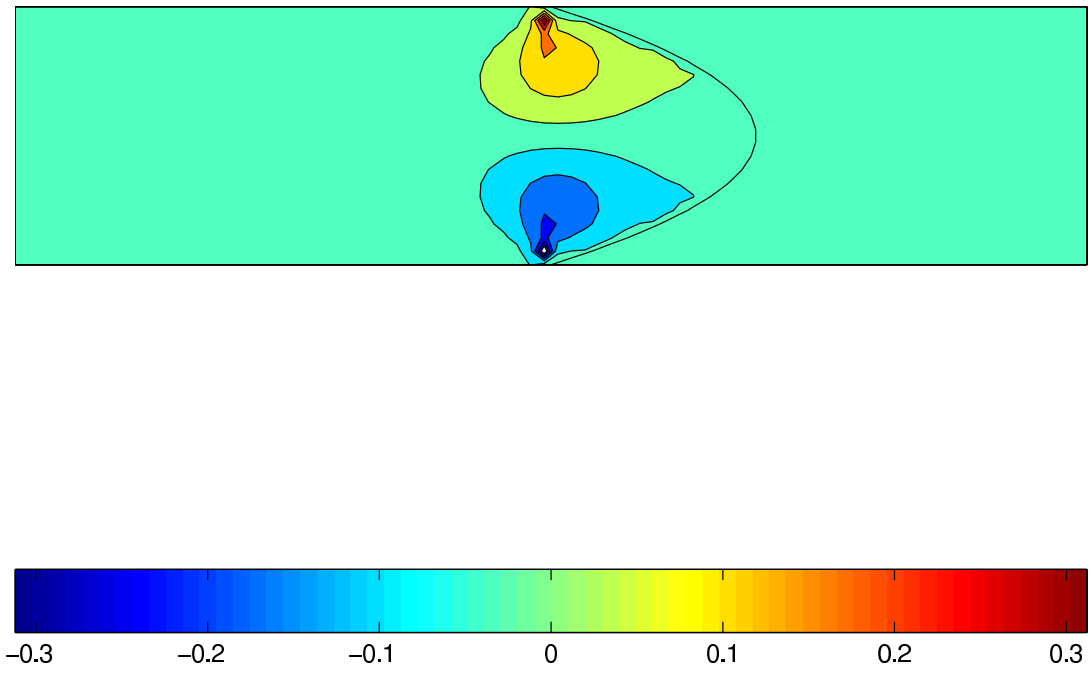

FIGURE 4.3: v computed on an 80×20 grid

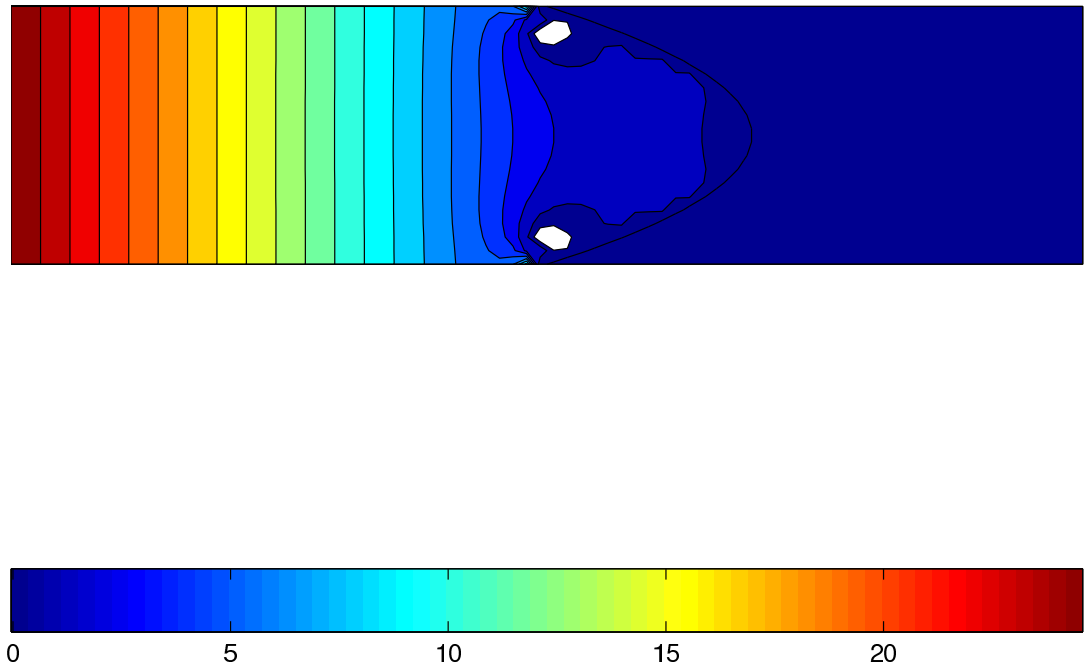

FIGURE 4.4: The pressure distribution computed on an 80×20 grid

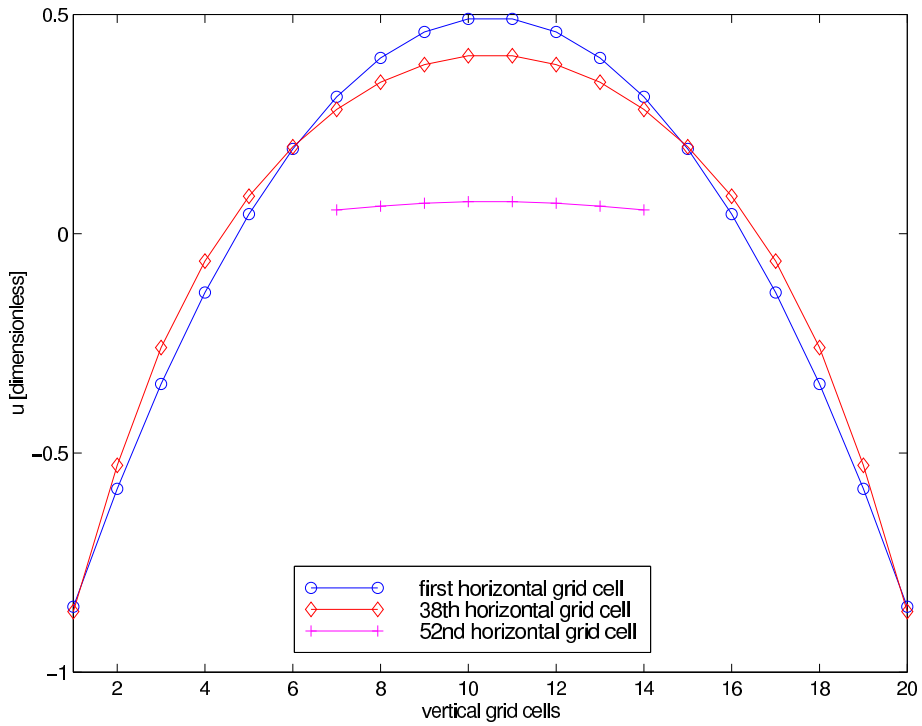

FIGURE 4.5: The evaluation of u on a 80×20 grid

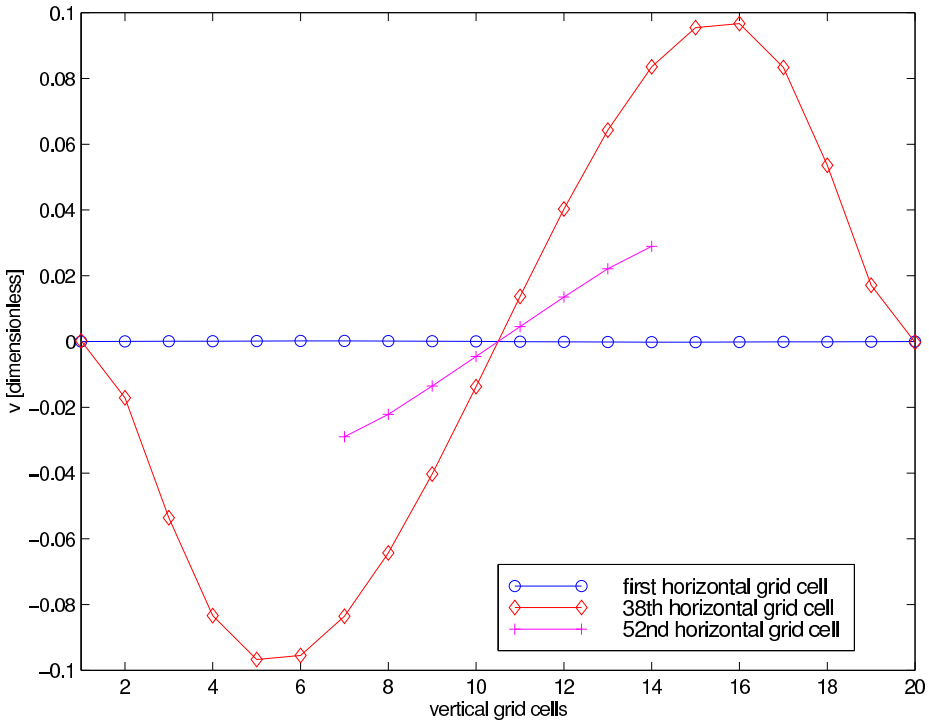

FIGURE 4.6: The evaluation of v on a 80×20 grid

distribution which is linear in x direction and constant in y direction, as they are typical for fully developed flow in a channel completely filled with liquid [17]. Figures 4.5 and 4.6 demonstrate the evaluation of u and v, respectively, away from a typical channel flow velocity field at the 'inflow' boundary. The Figures feature values at the 'inflow', in the vicinity of the moving contact line, and beyond the moving contact line (where the liquid domain does no longer fill the whole channel, see Figures 4.1 – 4.4). Furthermore, in Figure 4.1 we can clearly see the 'rolling' motion of the liquid onto the solids which is one of the main features of Shikhmurzaev's theory.

4.2 On a 160×40 Grid

Let us now compare the results from Section 4.1 with results achieved on a much finer grid. Therefore, Figures 4.7 – 4.12 show the results computed on a 160×40 grid. This time, the whole simulation took 402 'time' iterations, and the 'time' step computed with (3.27) was $\delta t = 1.4 \cdot 10^{-4}$, again constant, but only one fourth of the 'time' step size on the coarser 80×20 grid.

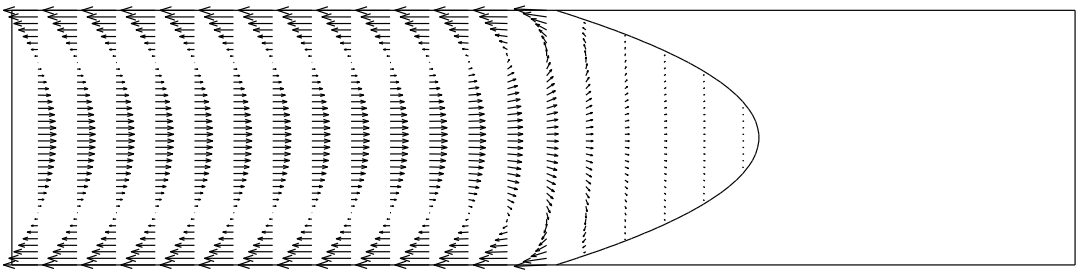

FIGURE 4.7: The velocity field computed on a 160×40 grid

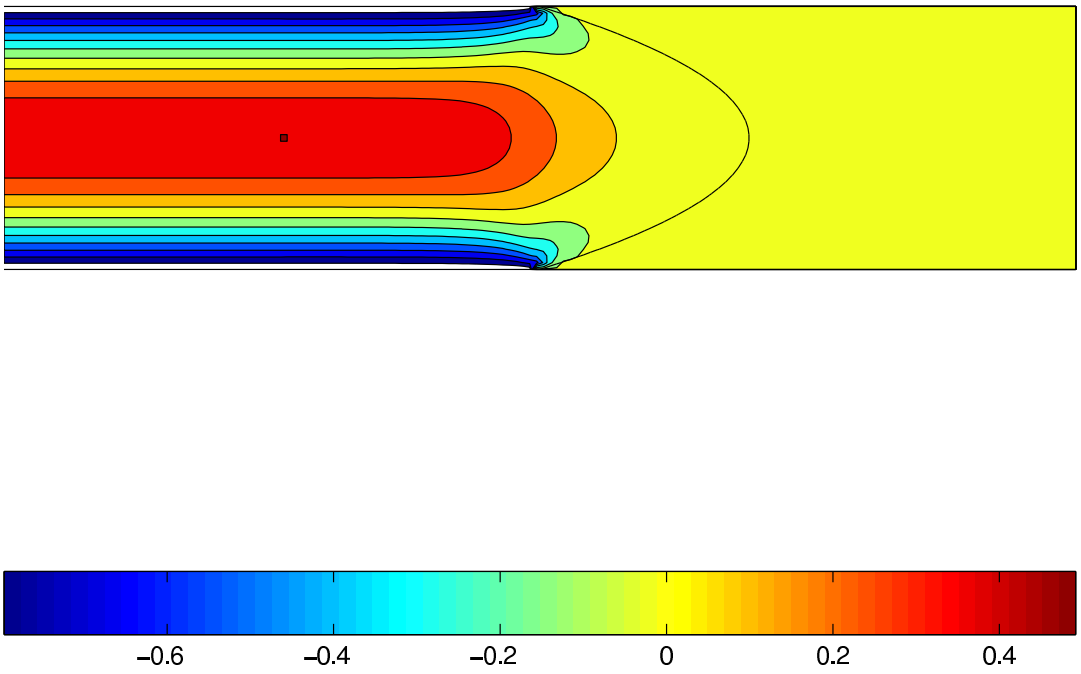

FIGURE 4.8: u computed on a 160×40 grid

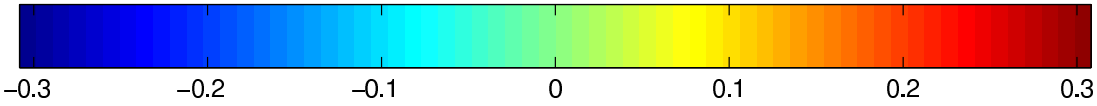

FIGURE 4.9: v computed on a 160×40 grid

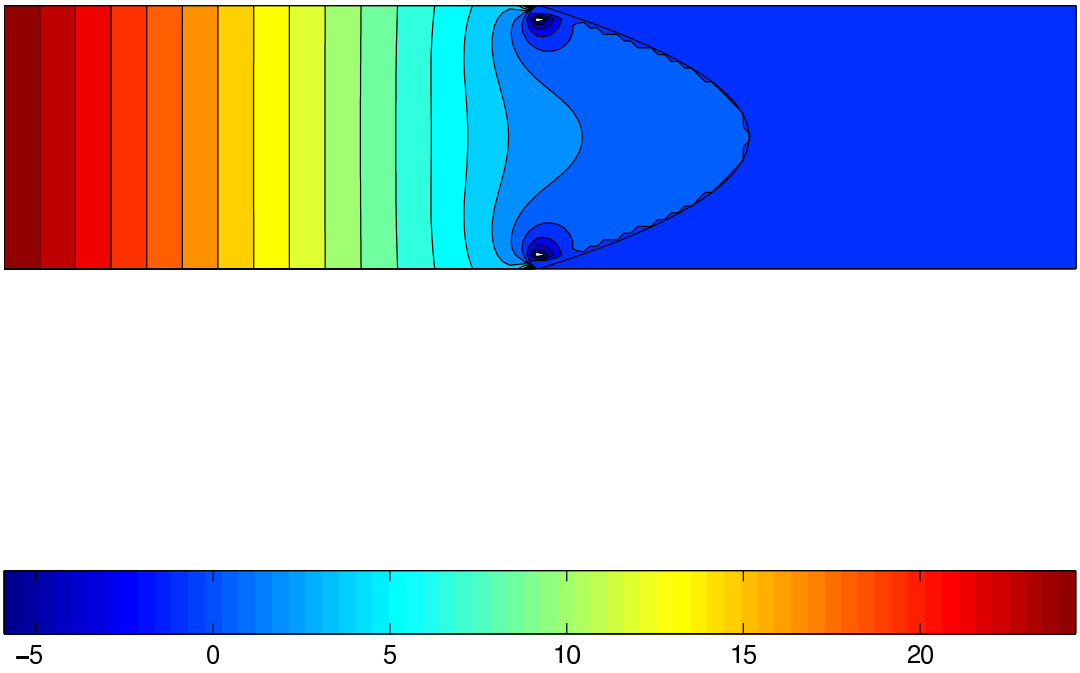

FIGURE 4.10: The pressure distribution computed on a 160×40 grid

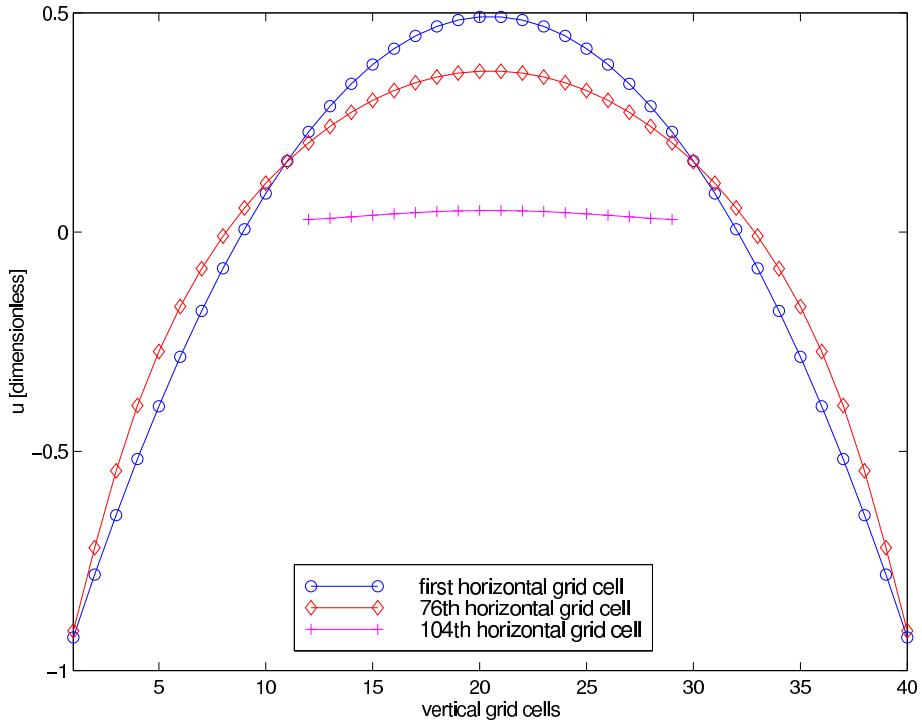

FIGURE 4.11: The evaluation of u on a 160×40 grid

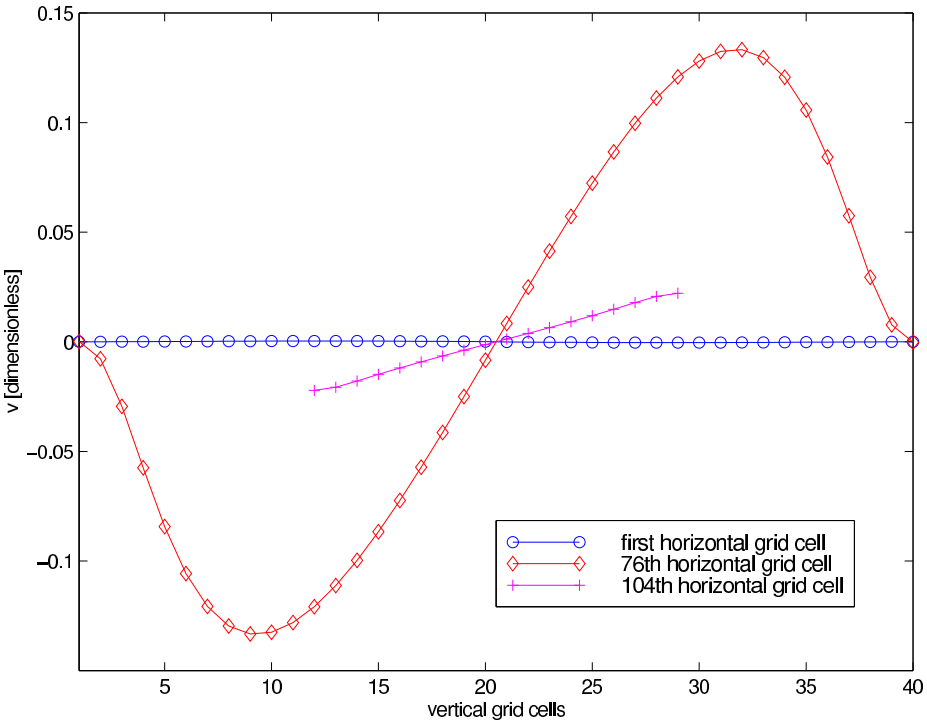

FIGURE 4.12: The evaluation of v on a 160×40 grid

Grid Size	'Time' Step Size	Number of Iterations
40×10	$2.3 \cdot 10^{-3}$	44
60×15	$1.0 \cdot 10^{-3}$	84
80×20	$5.6 \cdot 10^{-4}$	134
120×30	$2.5 \cdot 10^{-4}$	256
160×40	$1.4 \cdot 10^{-4}$	402
240×60	$6.5 \cdot 10^{-5}$	741
320×80	$3.5 \cdot 10^{-5}$	1114
20×20	$1.1 \cdot 10^{-3}$	78
30×30	$4.7 \cdot 10^{-4}$	152
40×40	$2.6 \cdot 10^{-4}$	243
60×60	$1.2 \cdot 10^{-4}$	460
80×80	$6.6 \cdot 10^{-5}$	709
50×8	$2.0 \cdot 10^{-3}$	49
75×12	$9.1 \cdot 10^{-4}$	94
100×16	$5.1 \cdot 10^{-4}$	148
150×24	$2.3 \cdot 10^{-4}$	279
200×32	$1.3 \cdot 10^{-4}$	436

TABLE 4.1: Data from computations on different grids

4.3 The Behaviour of the Numerical Method

The aim of this section is to discuss some observations made during the performing of the numerical experiments. Those observations might be a basis for the derivation of some general rules for the behavior of the numerical method discussed in Chapter 3, but we do not consider the detailed derivation of such rules in this thesis; we just want to give some first impressions of what could be possible. Therefore, the author collected some data from computations on several grids. These data are shown in Table 4.1. Please note that the 'time' step size δt is constant for any given grid. This might be a hint that stability condition 3.23 (whose right hand side is independent of 'time') dominates 3.21 and 3.22 (whose right hand sides depend on 'time').

The first part of Table 4.1 features data from computations on grids with quadratic cells, i.e. $\delta x = \delta y$ and therefore $i_{max} : j_{max} = 4 : 1$, the second part gives data for grids where $\delta x : \delta y = 4 : 1$ and therefore $i_{max} = j_{max}$, and the third part presents data for $\delta x : \delta y = 16 : 25$ and therefore $i_{max} : j_{max} = 25 : 4$. It is visible from Table 4.1 that, if we double i_{max} and j_{max}, the 'time' step size δt reduces to approximately one fourth of its previous value, and the program needs about three times as many 'time' iterations as before. However, on two grids with the same number of cells but different structures, δt and the number of 'time' iterations are not the same. For example, 80×20, 40×40, and 100×16

grids have 1600 grid cells each, but δt and the number of 'time' iterations are different for any two of those three. Anyway, on grids from the third group, δt is always slightly smaller and the number of 'time' iterations is always slightly higher than on the corresponding grid from the first group. This might happen because the shape of the single grid cells is fairly similar in these two groups (if we ignore the different orientation, of course).

Chapter 5

Concluding Remarks

5.1 What Could Be Done

In this thesis, we investigated a recently published theory for flow in the vicinity of moving contact lines. In its general formulation, this theory is very complicated but in the case $Re, Ca, \epsilon \to 0$, it can be considerably simplified by means of matched asymptotic expansion. To apply those means, we had to split up the spatial domain in three different asymptotic regions and were in fact able to get an analytical solution of the problem in the 'outer' asymptotic region and a problem formulation which is fairly easy to implement in the 'intermediate' region. Furthermore, we found that the dimensions of the 'inner' asymptotic region are neglectable as $Ca \to 0$, and we obtained a formula for the computation of the dynamic contact angle θ_d. Using this knowledge, we were able to compose a numerical method for the simulation of a channel inflow with $Re, Ca, \epsilon \to 0$. Therefore, we modified the public domain code NaSt2D in such a way that it iterates the Stokes equations in 'time' until the solution reaches its steady state. We decided to define the 'intermediate' asymptotic regions to be exactly the grid cells containing the moving contact lines on both solids, while the rest of the computational domain forms the 'outer' region. Furthermore, we implemented the formula for the computation of θ_d, and we prescribed the liquid front in such a way that it forms exactly the angle θ_d with each of the solids. With this numerical method, we were able to achieve reasonable results on a wide variety of computational grids.

5.2 What Could not Be Done

The numerical method presented in this thesis is only valid in the case $Re, Ca, \epsilon \to 0$, and those are in fact very strong restrictions: $Re \to 0$ and $Ca \to 0$ are not true for most flow systems, and ϵ is no longer small as soon as $l = U\tau = O(L)$. Furthermore, we can not treat real time–dependent problems with the numerical

method presented in this thesis. The restriction to time–independent problems with $Re \to 0$ is due to the fact that the model equations for flow in the slip region depend on the 'inner' limit of the 'outer' solution, and this limit is only known for time–independent flows with $Re \to 0$, the limitation to $Ca \to 0$ was made to keep the treatment of the boundary conditions for the slip region as simple as possible, and if ϵ becomes too large, the whole asymptotic analysis performed in Chapter 2 is no longer possible. Even though it is very desirable to have a numerical method for the simulation of a time–dependent channel inflow, the development of such a method is beyond the purpose of this thesis, and therefore it is left for future work.

Appendix A

Notations

This is a summary of all important notations used in this thesis except those that appear only in a short paragraph after their definition in the text. As general rules, boldface Latin letters denote vectors, boldface capital Latin letters denote matrices, and italic Latin letters as well as Greek letters denote scalar quantities. Furthermore, the superscript s denotes surface quantities, the superscript (n) denotes values after n 'time' steps, and the subscript i, j denotes values in grid cell (i, j). The notations are split up in operators (section A.1) and symbols (section A.2).

A.1 A List of Operators

Let us first give a list of some important operators used in this thesis. In the following table, $\mathbf{a}$ and $\mathbf{b}$ denote arbitrary vectors, $\mathbf{A}$ stands for an arbitrary matrix, and ξ represents an arbitrary co–ordinate.

$\mathbf{a} \cdot \mathbf{b}$	The Euclidean scalar product of $\mathbf{a}$ and $\mathbf{b}$
$\mathbf{A} \cdot \mathbf{a}$	The Euclidean matrix–vector product of $\mathbf{A}$ and $\mathbf{a}$
$\mathbf{a} \cdot \mathbf{A}$	The Euclidean vector–matrix product of $\mathbf{a}$ and $\mathbf{A}$
$\mathbf{a} \otimes \mathbf{b}$	The dyadic product of $\mathbf{a}$ and $\mathbf{b}$
$\mathbf{a} \times \mathbf{b}$	The vector product of $\mathbf{a}$ and $\mathbf{b}$
$\mathbf{a} \cdot \mathbf{n}$	The inner normal component of $\mathbf{a}$
$\mathbf{a} \cdot (\mathbf{I} - \mathbf{n} \otimes \mathbf{n})$	The tangential projection of $\mathbf{a}$
$\mathbf{a}^T$	The transposed vector of $\mathbf{a}$

$\frac{\mathrm{d}}{\mathrm{d}\xi}$	The total derivative with respect to ξ
$\frac{\partial}{\partial\xi}$	The partial derivative with respect to ξ
$\frac{\partial^2}{\partial\xi^2}$	The second partial derivative with respect to ξ
∇	The nabla operator
$\nabla\xi$	The gradient of ξ
$\nabla\mathbf{a}$	The vector gradient of $\mathbf{a}$
$\nabla\cdot\mathbf{a}$	The divergence of $\mathbf{a}$
$\nabla\cdot\mathbf{A}$	The matrix divergence of $\mathbf{A}$
$\nabla\times\mathbf{a}$	The curl of $\mathbf{a}$
$\triangle$	The Laplace operator ($\triangle = \nabla\cdot\nabla$)

A.2 A List of Symbols

In the following table, the reader will find some important symbols used in this thesis. Those that are only shortcuts are provided with a repetition of their exact mathematical definition.

a	The domain length in x direction
A	$= \alpha\beta$ ($= 1/12$ for channel flow)
α	A phenomenological coefficient
b	The domain length in y direction
B	$= -\frac{1}{1-\rho_f^s}\left(\rho_s^s + \rho_f^s u_{r(0)}(\theta_d)\right)\left(\frac{q}{4V^2}+1\right)^{-1}$
β	The coefficient of sliding friction
Ca	The capillary number $\left(Ca = \frac{\mu U}{\sigma}\right)$
δt	The 'time' step size
δx	The step size in x direction
δy	The step size in y direction

ϵ_1	The stopping parameter for the relaxation iterations
ϵ_2	The stopping parameter for the pressure correction
ϵ_3	The stopping parameter for the computation of the dynamic contact angle θ_d
ϵ	$= \frac{l}{L} = \frac{U\tau}{L}$
$F_{i,j}^{(n)}$	$= u_{i,j}^{(n)} + \delta t \left(\frac{u_{i+1,j}^{(n)} - 2u_{i,j}^{(n)} + u_{i-1,j}^{(n)}}{(\delta x)^2} + \frac{u_{i,j+1}^{(n)} - 2u_{i,j}^{(n)} + u_{i,j-1}^{(n)}}{(\delta y)^2} \right)$
Φ	The level set function
$\Phi_{i,j}$	The value of Φ at the center of cell (i,j)
$G_{i,j}^{(n)}$	$= v_{i,j}^{(n)} + \delta t \left(\frac{v_{i+1,j}^{(n)} - 2v_{i,j}^{(n)} + v_{i-1,j}^{(n)}}{(\delta x)^2} + \frac{v_{i,j+1}^{(n)} - 2v_{i,j}^{(n)} + v_{i,j-1}^{(n)}}{(\delta y)^2} \right)$
γ	A phenomenological coefficient
Γ	The boundary of the computational domain Ω
Γ_{in}	The 'inflow' part of Γ
Γ_{out}	The 'outflow' part of Γ
Γ_{solid}	Those parts of Γ adjacent to the solids
i	The cell counter in x direction
i_{max}	The number of inner cells in x direction
$\mathbf{I}$	The unit tensor
j	The cell counter in y direction
j_{max}	The number of inner cells in y direction
k_{max}	The maximum number of iterations for the pressure correction
κ	The curvature of the free liquid surface
l	The relaxation length ($l = U\tau$)

L The characteristic length of the flow system
(for channel inflow: the diameter of the channel)

λ $= \frac{\gamma\rho_0^s}{\sigma} = \frac{1}{1-\rho_f^s}$

μ The viscosity of the liquid

n The 'time' step counter

$\mathbf{n}$ The inner normal vector to a given liquid boundary

ν The security factor for the computation of δt

ω The relaxation factor for the SOR method

Ω The computational domain $\left(\Omega = [0,a] \times [0,b] \in \mathbb{R}^2\right)$

p The pressure

$p^{(n)}$ The value of p after n 'time' steps

$p_{i,j}$ The value of p at the center of grid cell (i,j)

p^s The surface pressure

p_S^s The reacting force component acting on the contact line
element tangential to the solid surface from the solid

$\mathbf{P}$ The stress tensor of the liquid $\left(\mathbf{P} = -p\mathbf{I} + \mu\left(\nabla\mathbf{u} + (\nabla\mathbf{u})^T\right)\right)$

$\mathbf{P}^s$ The stress tensor at the free liquid surface $(\mathbf{P}^s = -p^s(\mathbf{I} - \mathbf{n} \otimes \mathbf{n}))$

$\Psi_{(0)}$ The stream function in the 'outer' region

q $= \frac{2V}{\rho_s^s}\left(\sqrt{V^2 + \rho_s^s} - V\right)$

r The radial component in a (plane) polar co–ordinate frame

Re The Reynolds number $\left(Re = \frac{\rho UL}{\mu}\right)$

ρ The density of the liquid

ρ^s The surface density of the liquid

ρ_0^s	The surface density of the liquid corresponding to zero surface pressure
ρ_f^s	The equilibrium surface density of the liquid at the free surface
ρ_s^s	The equilibrium surface density of the liquid at the solid surface
σ	The equilibrium tension of the free liquid surface
t	The 'time' variable
τ	The surface tension relaxation time
θ	The angular component in a (plane) polar co–ordinate frame
θ_d	The dynamic contact angle
θ_s	The static contact angle
θ_{max}	The limiting contact angle of the flow system
u	The velocity component in x direction
$u^{(n)}$	The value of u after n 'time' steps
$u_{i,j}$	The value of u at the mid point of the right edge of grid cell (i,j)
u_r	The radial velocity component in the slip region
$u_{r(0)}$	The radial velocity component in the 'outer' region
$u_{r(0)}(\theta_d)$	$= \frac{\sin\theta_d - \theta_d\cos\theta_d}{\sin\theta_d\cos\theta_d - \theta_d}$
u_θ	The angular velocity component in the slip region
$u_{\theta(0)}$	The angular velocity component in the 'outer' region
$\mathbf{u}$	The velocity of the liquid
$\mathbf{u}^{gas}$	The velocity of the gas at the free liquid surface
U	The characteristic speed of the flow system, chosen here to be the speed of the solid(s)
$\mathbf{U}$	The velocity of the solid

v	The velocity component in y direction
$v^{(n)}$	The value of v after n 'time' steps
$v_{i,j}$	The value of v at the mid point of the upper edge of grid cell (i, j)
v_r^s	The radial component of the surface velocity
v_θ^s	The angular component of the surface velocity
$\mathbf{v}^s$	The surface velocity
V	$= U\sqrt{\frac{(1-\rho_f^s)\tau\beta}{\sigma(1+4\alpha\beta)}}$
x	The first component in a Cartesian co–ordinate frame
x_{mcl}	The x value of the moving contact line(s)
y	The second component in a Cartesian co–ordinate frame
z	The third component in a (spatial) Cartesian co–ordinate frame

Bibliography

[1] D. Bedeaux, A. M. Albano, and P. Mazur, *Boundary conditions and non–equilibrium thermodynamics*, Physica, A82 (1976), pp. 438–462.

[2] T. D. Blake, A. Clarke, and K. J. Ruschak, *Hydrodynamic assist of wetting*, AIChE Journal, 40 (1994), pp. 229–242.

[3] T. D. Blake and K. J. Ruschak, *A maximum speed of wetting*, Nature, 282 (1979), pp. 489–491.

[4] R. G. Cox, *The dynamics of the spreading of liquids on a solid surface.part 1. viscous flow*, Journal of Fluid Mechanics, 168 (1986), pp. 169–194.

[5] P. Deuflhard and A. Hohmann, *Numerische Mathematik*, deGruyter, Berlin, 1991.

[6] NaSt2D is available via anonymous ftp at ftp.lrz–muenchen.de/pub/science/fluiddynamics/cfd/NaSt2D/.

[7] M. Griebel, T. Dornseifer, and T. Neunhoeffer, *Numerische Simulation in der Strömungsmechanik*, Vieweg, Braunschweig, 1995.

[8] E. B. Gutoff and C. E. Kendrik, *Dynamic contact angles*, AIChE Journal, 28 (1982), pp. 459–466.

[9] L. D. Landau and E. M. Lifschitz, *Lehrbuch der Theoretischen Physik*, vol. VI (Hydrodynamik), Akademie–Verlag, Berlin, third ed., 1978.

[10] H. K. Moffat, *Viscous and resistive eddies near a sharp corner*, Journal of Fluid Mechanics, 18 (1964), pp. 1–18.

[11] R. Schwarz, *Numerische Mathematik*, Teubner, Stuttgart, fourth ed., 1997.

[12] J. A. Sethian, *Level Set Methods*, Cambridge University Press, Cambridge, UK, 1996.

[13] Y. D. Shikhmurzaev, *The moving contact line on a smooth solid surface*, International Journal of Multiphase Flow, 19 (1993), pp. 589–610.

[14] ——, *Dynamic contact angles and flow in vicinity of moving contact line*, AIChE Journal, 42 (1996), pp. 601–612.

[15] ——, *Moving contact lines in liquid / liquid / solid systems*, Journal of Fluid Mechanics, 334 (1997), pp. 211–249.

[16] M. Sussman, P. Smereka, and S. Osher, *A level set approach for computing solutions to incompressible two–phase flow*, Journal of Computational Physics, 114 (1994), pp. 146–159.

[17] F. M. White, *Viscous Fluid Flow*, McGraw–Hill, New York, second ed., 1991.

I hereby declare that I have done this thesis by myself and that I have not used any other resources than those indicated.

Kaiserslautern, 9th November 1998

Dirk Kehrwald